

*sam-sam id yuvase vrsann agne visvany arya a |idas pade sam idhyase sa no vassuny a bhara ||
sam gachadhvam sam vadadhvam sam vo manamsi janatam |deva bhagam yatha purve samjanana upasate ||
samano mantrah samitih samani samanam manah saha cittam esam |samanam mantram abhi mantraye vah samanena
vo havisa juhomi ||*

samani va akutih samana hrdayani vah |samanam astu vo mano yatha vah susahasati || RigVeda

“Sam” means resonance, Vedas suggest that an eternal vibration called “Bramhan” came out of Golden Womb (Hiranya Garva), Chitta~ means consciousness feelings, Manan~ the vibrations of consciousness

It is all about resonance, our consciousness feelings resonate with that of the supreme consciousness. When the touch of all connected hearts vibrates together, those vibrations confluence when the passions in every single consciousness units run deep inside their heart, when originally the vibrations of consciousness reside. May you move in harmony, speak in one voice; let your minds be in agreement; just as the ancient gods shared their portion of the sacrifice. May our purpose be the same; may we all be of one mind. In order for such unity to form I offer a common prayer. May our intentions and aspirations be alike, so that a common objective unifies us all.

8 Hinductor Not Memristor— Synthesis of Atoms and Crystals Made of Magnetic Light

8.1 IT IS RESISTANCE FOR VORTEX ATOMS BUT NOT FOR ELECTRONS

The 3D topological pattern of a very weak magnetic field plays a fundamental role in governing the formation of a star (Pattle et al., 2018). Weak magnetic fields are there everywhere in the biological system, now even the magnetic field around a single atom has been measured (Willke et al., 2019). The electric field has a monopole as positive or negative charge; one can isolate positive and negative charge separately. The magnetic field does not have such a provision. Once the debate regarding the supremacy of electric field over the magnetic field was settled in the 1820s by Lord Kelvin, no one questioned why the current flow that is fundamental to the electric field is required to generate a magnetic flux, why not the phase flow alone builds a magnetic flux that is an integral part of a magnetic field. There are plenty of reports of generating magnetic flux by flowing current, it is a must to happen, regulating magnetic phase, spin flow, magnetic wave flow, everything could be easily feasible following the guideline of Maxwell’s law (Matsukura et al., 2015; Stöhr et al., 2009; Lottermoser et al., 2004; Henke et al., 1981; Figure 8.1a). There has been an attempt to change the electric polarization vector or phase using magnetic phase (Ishiwata et al., 2008).

Electric field controlling the magnetic field could easily be realized. However, the electron would not flow, yet the magnetic flux would flow appeared not possible unless one discovers the magnetic monopole. Instead of a magnetic monopole, it is easy to build, magnetic vortex atom and do similar work, as it is done for Hinductor.

So, an electric charge has to move, and only then a magnetic field is generated. The quest for a magnetic monopole started long ago (Dirac, 1931), when Dirac argued for a unique magnetic monopole. Giant accelerators tried to find a monopole fundamental to the universe, but failed. Now, the lattice defect-induced vortex of a magnetic field is found to mimic the magnetic ring. Vortices could happen in a small excitable media like a time crystal (Winfree, 1986b, 1990, 1994). Spiral features can take us to use the topological feature, and that enables using the negative refractive index (Pendry, 2004). Supramolecular springs and ratchets have an intimate relationship (Mahadevan and Matsudaira, 2000), and entropic effects do play a fundamental role in the composite dynamics. It should be noted that for computing or decision-making, this might not be essential. One recent course of historic development started when rotational angular momentum was introduced to light; here, it would be a journey to the universalization of angular momentum of light.

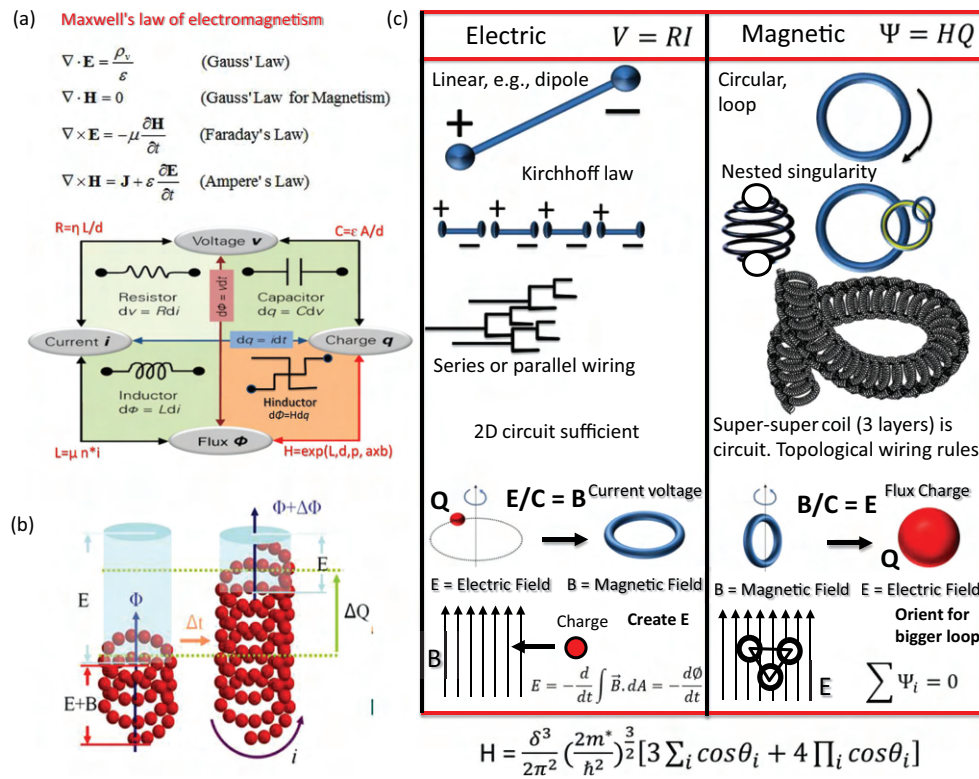


FIGURE 8.1 (a) Maxwell's equations (top) and a table for missing fourth-circuit element, a new symbol for H-Hinductor device different from Memristor. (b) The schematic of the device for the fourth-circuit element, change in the stored charge reflects in the change in produced magnetic flux. (c) A table is comparing the world of electronics and the world of magnonics, if magnetic particle an equivalent to charge is found using vortex atoms proposed by Kelvin.

Why do we need fourth-circuit element: Memristor is not the fourth-circuit element: No brain component should use significant energy; if we do, then the integration of 100 billion devices would require megawatts of a power supply. Considering all critical limits, one could find that we need to confine power expenditure of entire human brain hardware within a few kilo-watts and, therefore, the power consumption in a single neuron equivalent device cannot be more than a few nano-watts or microwatts. Such a frequency-fractal processor device was proposed in 2014 (Ghosh et al., 2014a). One has to invent a fractal-processing device, that generates time crystal with quaternion, octonion, and dodecanion features, and for that purpose, we start with the fourth-circuit element. In the 1870s, three basic electronic devices the capacitor, inductor and resistors were known. Leon Chua was the first to notice that by symmetry argument magnetic flux and the stored charge should be linked by an unprecedented device, he called it memristor (Chua, 1971; Figure 8.1b). Memristor is not a fourth-circuit element; any device that created the biggest sensation in the world in 2008 (Strukov et al., 2008), to realize cannot generate magnetic flux is not a fourth circuit element. Chua himself wrote in 1971s seminal paper that all memristor properties could be derived using inductor L, capacitor C, and resistor R. Hence memristor, even one goes by the view of the main proposer is not a fundamental circuit element. Moreover, since all properties of memristor,

memcapacitor, and meminductor (Di Ventra and Pershin, 2013) could be derived using conventional circuit elements, one cannot consider this as a fundamental element at all. In contrast, no combination of primary circuit elements could generate the electronic properties of the fourth-circuit element. Therefore, it is unique. The missing memristor remains unfound despite thousands of follow-up articles.

The paradox of fourth-circuit element: Why memristor could be an inductor but never a fourth-circuit element: The proposal for the fourth-circuit element has a paradox (Figure 8.1b). If an electric current flow for linearly changing the magnetic flux, then it is an inductor, no more a fundamental circuit element. On the other hand, if the charge does not move yet, a magnetic flux is produced, and then Maxwell's law described in Figure 8.1a violates. Universalizing Dirac's classic 1931 charge-flux quantization holds an answer to this paradox—if Dirac strings are spiral, magnetic monopoles could survive together even in ambient atmospheric condition. Resolving the paradox using a generic magnetic pole generator would open the door to building usable practical devices (Figure 8.1c). We suggest getting out of the intense quest to find a universal magnetic charge as a fundamental particle and limiting the quest to finding a free particle-like magnetic entity ($B \gg E$) that does not require an accelerating charge and does not require an external massive magnetic field to observe. Further qualification of such free particle-like

structures would be (i) self-assembly of these magnetic particles would generate more magnetic field like an electric charge, (ii) generation of electric charge by rotation of magnetic particle, and (iii) rotational direction of a field like spin.

Knots of darkness generated by a coil, a supercoil, a super-super coil is tubule-morphic, not neuromorphic:

When we look at a DNA molecule vertically from the top, it looks like a flower. The origin of flower shape is a twist in its spiral. There are two spirals superposed on each other, in summary it is a spiral of a spiral. The twist creates a mixed defect of an edge dislocation and a line dislocation on the cylindrical surface. DNA is not alone; α -helices in the protein, tubulin dimer, microtubule nanowire, several protein complexes hold such a unique twist in the spiral. One of the most significant advantages of using a helical geometry is that due to the geometric shape alone the spiral pathway quantizes signal, thenceforth filters noise. The ultra-low pitch spiral design allows several alternative spiral channels to operate simultaneous signals, the quantization of energy happens. Naturally, quantum effects generate in an ambient condition (Atanasova and Dandoloff, 2008). When we change the surface design, the optical signal falling on the surface would diffract and interfere; the resultant 3D pattern would carry a signature of that surface. One could see dark lines floating in the 3D space. In the optical vortex studies, these studies are done frequently. We state explicitly that in these lines, electric field $E = 0$. Really? No one ever checked whether or not Maxwell's equations are at all valid inside those dark lines. Someone should do it. We leave that and introduce the coil of coil of coils, or super-super coil. The α -helices of a tubulin monomer form a coil which generates three kinds of diffraction patterns.

Imagine a cylinder. On its surface, through an imaginary spiral, a set of dark lines along with dark rings are moving clockwise. On its surface through an imaginary spiral, hairpin-like shapes and dark ring are flowing counter-clockwise. On its surface longitudinally, super-super coils of dark lines (Nye, 1983) are moving. Thus, three coexisting dynamics are equivalent to three Bloch spheres. Each Bloch sphere has a great circle with singularity points on its perimeter. The singularity points in a circle constitute a geometric shape. Thus, DNA or α -helices like spirals are the smallest unit of information. Supercoil of α -helices is a tubulin dimer, and the super supercoil of α -helices is a microtubule. Thus, microtubule nanowire is a triplet of coils, and it is the smallest unit of the tubule-morphic device.

The background history of the magnetic vortices: If a semiconductor sandwiched between a pair of metal electrodes exhibits hysteresis and bistable states, one could flip between the two resistances like a switch, then it is memristor. Since current flow is allowed in Chua's memristor, one could make an inductor-like device and generate magnetic flux, too. However, if one remained strict to the definition and was determined to build a device that does not flow any current yet produces a magnetic flux, then several critical research fields of contemporary physics need to be bridged. However, if successful, magnetic resonance would enable using the negative

index of refraction (Valentine et al., 2008), super-lensing (Smith, 2004) and cloaking (Schurig et al., 2006). Magnetic wireless communication is superior to electrical communication as electrical signal does not diminish while passing through water, moisture and metal.

Moreover, a magnetic field penetrates most insulator materials. The barrier should have another specialty, an electromagnetic lensing effect that converts emitted electromagnetic burst into a magnetic one. A barrier or boundary of a key device element might play key roles in building noise-resistant protection (Figure 8.2a). There are multiple routes (Karaveli and Zia, 2010). Charge storage is controlled by resonance frequencies of input ac signal oscillating them coherently initiating an antenna like the radiation of magnetic ripples (Figure 8.2b, c). Even though the charges do not move out of the well, due to an extremely insulated matrix outside, they oscillate physically as a group (Figure 8.2c, d). Thus, Maxwell's law is not violated. Since the current does not flow, still a magnetic flux is produced; therefore, the device cannot be tagged as an inductor. The linear relation between stored charge and produced magnetic flux suggests that it is a fourth-circuit element, but one does not get any reasonable current-voltage characteristic as the memristor demands. In this fourth-circuit element, the electrical resistance is infinity, but another resistance, the ratio between flux and charge is 0.001, i.e., very low. Following suggestions of Chua, Sahu et al. have given their device a distinct identity, namely Hinductor, and assigned it in a different class than a memristor.

Electric vector is 10^4 times more than the magnetic vector: The model explored for the fourth-circuit element, is a helical wire made of dots that are a special kind of quantum well or traps. The well is so designed that the electric vector is perpendicular to its wall's surface and magnetic field vector is in the plane with the wall. The density of states of the virtual wall's 2D surface lenses the electric vector and adds a part of it to the magnetic vector. One to two orders magnetic field enhancement by confining electrons and then accelerating them through the depleted field created by surface topology is a reasonably well-understood phenomenon (Shan et al., 2001; Johnston et al., 2002a, 2002b; Figure 8.2c, d). A subtle change in the stored electron would change the topology of surface depleted field, thus, regulating the phase correlation of coherent emission from this well like nano-antenna (Biagioni et al., 2012; Michler et al., 2000). Both in the classical and the quantum systems, the emission survives only for a few picoseconds, until the coherent resonance burst survives. The phase space interaction suggests the formation of a spiral path (Figure 8.3a), optical axis ensures the purity of two interfering waves (Figure 8.3b, d). So, we arrange multiple wells in a 3D spiral arrangement (Empedocles et al., 1999; Figure 8.3c) so that the magnetic flux acquires a stable experimentally measurable standing wave. Interference on the spiral path could depict the signature of magnetic radiation distinctly from the electrical contribution (Freed and Weissman, 1941). Arrayed structure assists in enhancing the magnetic field (Cui et al., 2016). Imaging the magnetic flux has been a challenging task (Vignolini et al., 2010). Normally, magnetic vector interacts

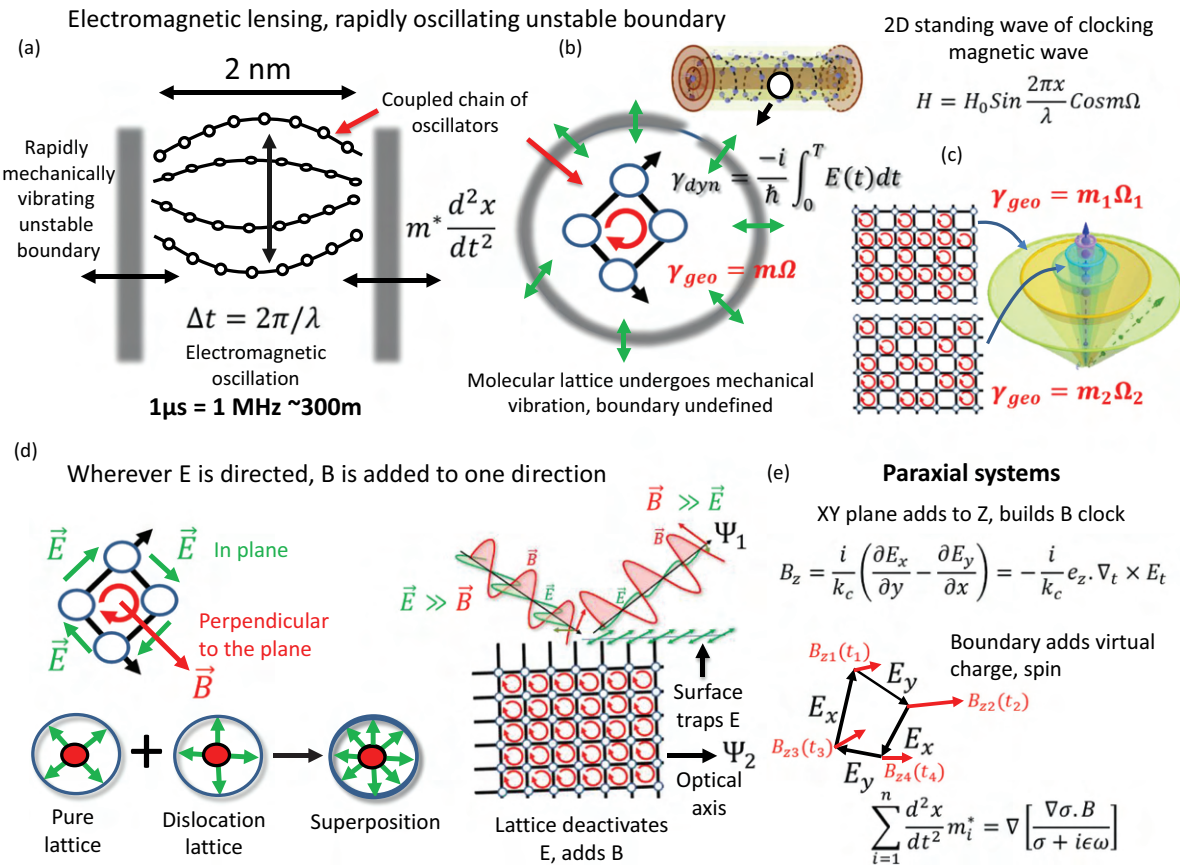


FIGURE 8.2 (a) How a rapidly vibrating membrane could hold a large waveform. Coupled chain of oscillators could generate a collective oscillation, quantum or classical. (b) Molecular helical array forming a vortex or nanotube builds a lattice on the nanotube surface (left). Here m is the magnetic quantum number, Ω , solid angle enclosed by the rotating field vector. Dynamic and geometric phases are isolated. (c) Periodically clocking wavefunction generating a geometric phase builds a standing wave. For different composition of charge distribution on the surface different cones are produced. (d) Magnetic vector (red) is perpendicular to the plane while electric vector is in plane with the cells. Dislocation rotates the plane of polarization and superposition of both should create a mixed polarization light, does not happen. The protocol to demonstrate $B \gg E$ from $E \gg B$ is shown. (e) How paraxiality works, electric E vectors transfer momentum to the magnetic B vector.

10^4 times less than the electric vector with the electrons of a sensor, so detecting a magnetic flux in the light has been a challenge, so metamaterials are used where conducting rings sense the magnetic flux rapidly (Schirber, 2010).

Topologically protected spin textures could be resonantly excited and its elliptical dynamics which contain anticlockwise and clockwise modes could be tuned by applying different frequencies of the microwave field (Figure 8.3a, e). The conversion between these two elliptical modes is achieved by a transition to linear vibration (Jin et al., 2017). One could do such phase modulation by applying THz pulses generated by surface depletion field. Infrared signals of 5–6 THz (~ 300 –320 K, little above room temperature) get frequency modulated to the lower THz regime 60–300 GHz, by the topology of the surface.

Do not look for a superconductor, look for super insulator: Since charges are not moving out of the quantum well, as if all the wells are floating in an infinite resistance or extremely insulating matrix, the charges formed inside the

well remain trapped (Figure 8.2b). In this scenario, the differential conductance, the key to almost all major electronics theory and experiments do not work,—sending a current or applying a voltage, returns no output. However, if a new differential, the relative variation of flux and charge, or differential flux-charge is measured, in some systems where its value is very low in spite of a nearly infinite resistance, a new type of communication could be found. Dimensions of differential conductance and differential flux-charge are the same. However, the physical significance is very different, while the first, is governed by collision and scattering of carriers (e.g., electrons, quasi-charge), for the later, the topology of charge-trap centers in the matrix of extreme insulators is the key (Figure 8.1c). While avoiding the collision and scattering have guided the ultra-low, noise-free quantum and classical adventures, the differential charge-flux has no such weakness. It means, one could in principle measure, quantum effects in ambient atmosphere, just like we do it in quantum optics. One has to measure three hallmarks of quantum,

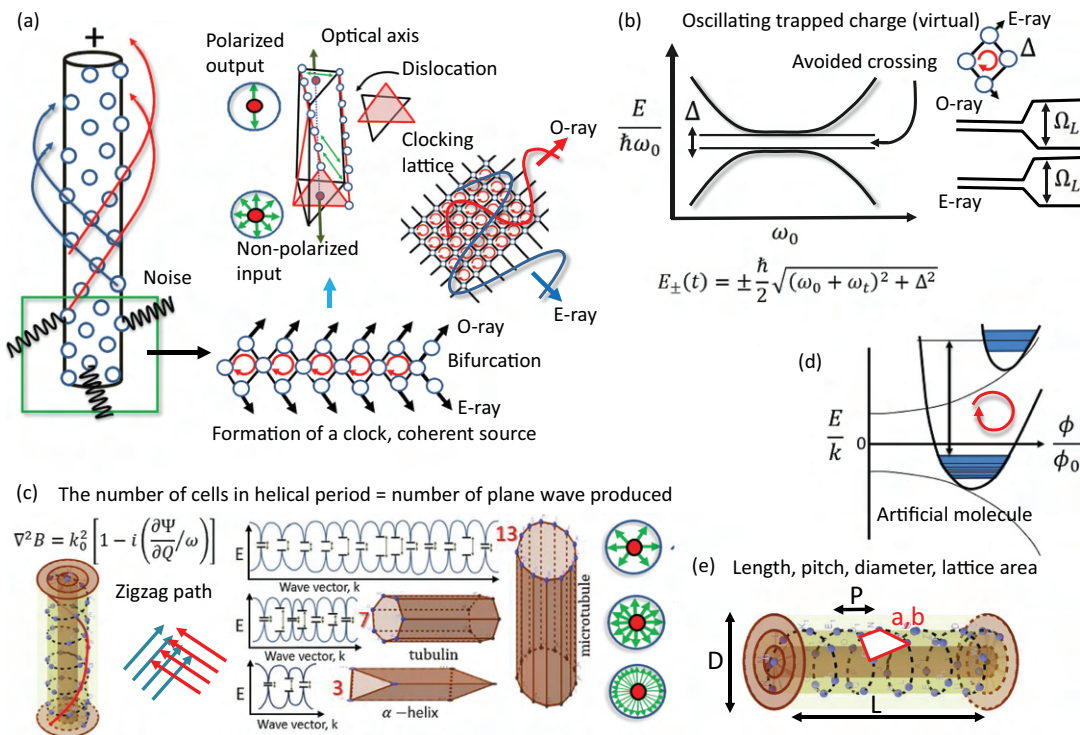


FIGURE 8.3 (a) All vortices or cylinders have a polarization direction. The noise is converted into a spiral organized signal and photons undergo O-ray and E-ray split triggered by dislocation, these are two coherent sources. Spontaneous generation of the polarized signal is shown. (b) Avoided crossing Δ splits virtually trapped charge. (c) The scheme shows α -helix with three centers of interaction per cylinder, tubulin with seven circuits or seven compositions of helices and finally 13 protofilaments. Polarization chart for 3, 7, and 13 are shown. The number of cells in the cross-section of a cylinder or vortex determines the number of the plane-polarized signal produced by the device. (d) Movement of system point in the configuration space of an H device. Here the configuration space is created by relative magnetic flux and the energy is normalized with respect to the wave vector. (e) Only four geometric parameters regulate the H property, Length, L, pitch P, diameter D, and lattice area a, b.

fractional quasi-charge, the ripples of a quantum well and the Fermi velocity (Lykken et al., 1970) which were thus far measured using the differential conductance, using differential flux-charge. Using them Sahu et al. estimated the magnetic flux and charge associated with the quantum capacitance and quantum inductance of a tubulin monomer; and accurately determined that no kind of wiring works for quantum elements. Sahu et al. verified the reliability of this new differential by building a theory, how quantum well emitted the magnetic rings interfere to form standing wave and then live to image the standing wave of magnetic flux. Its origin is a quantum antenna driven by oscillating charge trapped within that shapes the field correlations, emits a magnetic field at resonance, even if a single pair of tori interfere, the spiral standing waveforms.

8.1.1 QUANTUM NON-DEMOLITION: $e - \pi - \phi$ QUADRATIC SENSORS

Quantum demolition a historical perspective: Making the quantum analogs of classical electromagnetism laws, and everything that we find in the classical world has been a faithful practice for the quantum researchers for a long

time. No attempts were ever made to see what happens if the resistance that destroys the quantum coherence is increased critically arresting the motion of an electron. Critical environments often lead to quantum effects, but the laws prohibited us from seeing anything by arresting the electron flow critically. In a quantum world a quasi-particle wave can interfere without flowing electrons, the waves edit phase to exhibit unique topological resonance by quantum interference. Despite several attempts to safeguard information during measurement, it is still an open question whether it is at all possible to measure information without modifying or destroying natural weak vibrations. In the last 50 years all efforts to evade quantum demolition were optical (Braginsky, 1980; Sewell et al., 2013). Earlier, isolation was a route to make a device silent, e.g., “flux capacitor,” which was really a one-way optical loop for helping isolate sensitive quantum equipment.

Resistance-less paths for the clocks to transmit and doing mathematics: vibrate the cavity boundary for $e - \pi - \phi$: Flowing a charge through the resistance fewer paths has been the key to survive a quantum effect. It means that we do not want the carrier, be it electron, quasi-particles or photon to move out of the cavity, rather, remain trapped in the

cavity forever, do not even leak. So, we want super-insulators where the Fermi velocity of carriers is very low and which are vibrating mechanically. Due to the coupled vibrations among the cavity boundaries we get a mechanical rhythm. Periodic or clocking oscillation generates a magnetic field or a loop that absorbs more electric vectors in its plane. Thus, the necessity of clocks delivers a coupled electrical mechanical and magnetic rhythm leading to $e - \pi - \phi$. Similar to the electronic route, an alternate phase route could lead to a plethora of technologies to minimizing the resistance for the phase flow along the path, so that the magnetic field or magnetic flux carries the quantum information with null resistance just like the cooper pairs face in a superconducting material.

The development of a new kind of $e - \pi - \phi$ sensor: Normally, during the measurement of information in a material, the pump-probe technique is used. Even the day-to-day multimeters we use, it pumps a large bias to the device under test and then measures its response. Instead of pumping external energy to amplify enough to sense its response, one could envision a new thermo-magneto differential sensor that is tuned to interfere and modulate the geometric phases of magnetic flux waves produced at the atomic scale to the micro scale. The new culture of phase-based magnonics that might replace electronics in the coming future would rely on the coupled geometric resonance $e - \pi - \phi$. Imagine a futuristic world where instead of the multimeter that measures current-voltage we could have a cheap flux-charge meter. Most importantly we would not be pumping huge energy and then measure the outcry of the device under test. Synchronizing with the $e - \pi - \phi$ coupled oscillation requires a very small amount of energy that runs a search mode to find the right $e - \pi - \phi$ condition in a device, if that is done, then the new generation $e - \pi - \phi$ sensor would read the flux-charge properties like the inductance H without destroying the basic parameters. Instead of relying on the conventional electrical parameters like current or voltage, three simultaneous recordings allow reading the rate of change of flux as a function of charge directly in a pure form. Literature is rich with infrared sensors (Peng et al., 2015) and magnetic flux sensors (Shi and Li, 2011). When a fourth-circuit element Hinductor, H explores the geometry of a device so extensively, noise harvesting becomes natural and heat pipe effect often dominates the noise to signal conversion (Wang and Gundevia, 2013).

8.1.2 RAPIDLY OSCILLATING CELL MEMBRANE HOLDING A LONG WAVE

Classical waves can pick up geometric phase, exclusively preserved for quantum: Imagine a core-shell structure, where the boundary that makes a cavity have a different dielectric property than the filling material inside the cavity acting as a dielectric resonator. Boundary and inner structure vibrate very differently (Figure 8.2a). Hinductor coils (Figure 8.2b) are like single molecules, and the boundaries vibrate very slowly (kHz) than its internal core material, which vibrates at MHz or GHz, i.e., radio wave or

microwave frequencies. Thus, boundary and internal structure get energetically isolated. Even in a noisy environment, the boundary isolates unwanted input, makes internal rapidly vibrating structure into an adiabatic system. If the boundary vibrates periodically, then the wave function representing the internal structure would acquire a geometric phase in addition to a dynamic, phase. This wave could be a classical wave, so, at room temperature, ambient environment an electric, magnetic or mechanical wave could acquire geometric phase that was thought to be a prerogative of a quantum world (Lauber et al., 1994). How do we prove it? Check Aharonov-Bohm effect, i.e., where electromagnetic interference carries quantum information (Mead and Truhlar, 1979). In summary we get dynamic and geometric phase added to the electromagnetic signal passing through a molecular structure.

Electromagnetic, mechanical, and magnetic vibration of the membrane: Since 1930s, routinely measured protein vibrations (Vollmer et al., 2002; Zhai et al., 2000; Hanham et al., 2015) have failed to become a marker to detect the onset of a disease early, as subtle measurements flip a large number of its vibration modes. As protein vibrates at many different frequencies at a time, no probe exists to read multiple energy domains at once, classical markers cannot instantly detect fractional changes in the resonance frequencies caused by mutation or virus attack. To measure quantum capacitance and quantum inductance are quantum markers of geometric resonance of proteins are wavelike, means, originates purely from wave reflectance, transmittance and interference. So, a minute change in protein's local structural symmetry makes a significant change in phase. Earlier Sahu et al. reported significant changes in the resonance frequencies of microtubule as it becomes cancerous. Now, the same effect is read quantum mechanically to enhance the energy detection resolution to 10^{-21} eV, a new $e - \pi - \phi$ probe detects the subtle changes in the internal degrees of freedom, yet momentum conservation yields Planks constant repeatedly. Measurement is self-fault tolerant hence fit to dip in a living cell for the quantum detection of a disease at the very onset.

8.1.3 PARAXIAL SYSTEMS

A paraxial system means a transverse component of the electric vector contributes to the magnetic part of an electromagnetic wave stream (Figure 8.2e). Electric and magnetic vectors behave uniquely in a paraxial system (Berry, 2004). The device is a doublet or triplets of identical concentric cylinders of diameter D , length L , made of spirally arranged m nano-dielectric resonators in one helical period, with a total Ω number of quadrilateral lattice cells, each with sides a and b (Figure 8.3a). The spirals with pitch P , are further twisted by an angle δ . One cylinder with a 2D array of dielectric nanoparticles amplifies both E and B together, while two cylinders, each with an edge and screw defects at a relative angle α between the layers, create two distinct spatially isolated vortices, one electric ($E \gg B$) and the other

magnetic, $E \ll B$. For three layers, the knots change shape with time. Noise shifts the coils relative to each other, it tunes α , the angle between the overlapping dark lines, since coils are identical, noise initiates a beating which filters out E mixed in the dark B lines. A Fabry-Perot interferometer like set up was used to amplify B by infinite repeated reflections between the plane wave bender and the vortex lens. To see the ripples of magnetic vortices, move away from optical vortex, put a large $12'' \times 12''$ magnetic film to find the invisible magnetic vortex location, rotate the sample in a quartz cell to fine-tune the intensity of B in the vortex, keep the solution opacity at 60%, project it too far >5 m, do not use a lens to focus the vortex atoms, most spirals and fractals would give such vortex crystals.

The device operation follows two simultaneous steps. To write or erase a dynamic feature one has to send an ac signal $\hbar\omega$ to resonantly vibrate the surface cells, then shine a monochromatic polarized light to read the encoded information as a crystal of magnetic vortex. Quantum systems like vibrating molecules or nuclei, do not have fixed, but vibrating boundaries with momentum $m^*v = \nabla\phi$. This vibrating boundary adds a geometric phase ϕ to the trapped signal $\hbar\omega$. The trapped signal and the direct input signal interfere and give rise to Aharonov-Bohm effect at an ambient atmosphere. A very low-frequency signal ω_0 is born, the wavelength is far greater than the cell size ($a, b \ll \lambda$, paraxiality). Two events happen in parallel. The cell delays signal, oscillating walls build $\vec{\psi}_{trap}$, then emits $\vec{\psi}_{osc}$, finally builds $\vec{\psi}_{mag}$ globally on the cylinder surface. Since ($a, b \ll \lambda$), the deviation θ of \vec{E} vector is very low, i.e., $\sin\theta/\lambda \rightarrow \theta/\lambda$, the signal $\vec{\psi}_{mag}$ follows different spiral paths (anisotropy), distinct paths activate N vibrational modes. Thus, input high-frequency signal $\hbar\omega$, generates N very low-frequency signals ($\omega_1, \omega_2 \dots \omega_i, \omega_n$), as G-band, which interferes and creates distinct local density of states on the cylindrical surface, L, P, D and area ab sets the boundary condition for interference. Thus, in-plane \vec{E} vectors are consumed by the cells but the coupled G-modes with wave vectors k_i, k_{i+1} modulates ϕ as $\tan^{-1} k_{i+1}/1+k_i$, a precession $\pm\phi$ to the \vec{B} vector in those plane waves whose \vec{E} vectors lie along the cell plane (Figure 8.2e). For a mode i , all $\vec{B}(x, y) = \vec{B}\cos\phi$ vectors perpendicular to the cylindrical surface delivers an average sum of magnetic flux $\langle \vec{B}(x, y) \rangle$. Thus, plane-polarized light shined on a cylinder acquires coupling coefficient CC_i of all vibrational modes activated by $\hbar\omega$, in its B vector. Modes are visible in the quantum tunneling images.

8.1.4 ANISOTROPY AND AVOIDED CROSSING

Planar chiral structures automatically develop an anisotropy in the propagating electromagnetic, asymmetric structures even split the electromagnetic wave (Fedotov et al., 2006).

Engineering artificial dressed states: Say we draw a set of parallel lines (Figure 8.3a). Then, another set of parallel lines crossing the other. At the junctions we keep an element that stores charge or delays the motion of charge passing through the matrix. If we build a cylinder by arranging and

spiraling balls, we can create several cross-bar patterns on the surface. The most interesting part is that the flowing charges dwell for a longer time along the parallel paths, it is analogous to trapping a charge. We do not restrict what would be the charge, could be a quasi-particle, or an elementary particle, it is the designer's choice. The question is to control these states. The energy between two levels

$$E_{\pm} = \frac{\hbar}{2} \sqrt{\omega_0^2 + \omega_t^2 + \Delta^2} \quad (8.1)$$

with an energy gap Δ (Figure 8.3b). On a spiral cylinder, if there are different types of parallel paths, each set of paths have a distinct resonance frequency ω_0 , and applied energy E_{ac} generates a signal ω_t . Here n number of quanta is exchanged continuously between E_{\pm} , even without any metallic layer $H = E_{ac}(n_1^2 + n_2^2 + \dots + n_n^2) \dots$ H1. Thus, at around the resonance frequency, we get dressed states, i.e., the wave vector $k = 2\pi/\lambda$ oscillates periodically ($\cos k$), following

$$E_{\pm} = \sqrt{2(1 - \cos k)} \quad (8.2)$$

hence we get a periodically oscillating band gap (Figure 8.3d), the wave vector K^* switches between elliptical and circular polarization. Consequently, the basic definition of cavity resonance or dielectric resonance is not valid here. External noise activates the cells in the crossbar pattern, but external ordered signals disrupt natural communication between clocks. Even using the term resonance is not valid in strict terms. The crossbar trap's dimension d does not decide vibrational clocking frequency of trapped charge, in fact, $\lambda \gg d$. The particular condition, $\lambda \gg d$, transverse components of electromagnetic wave contributes to the longitudinal component. The light or electromagnetic wave of any frequency range would experience magnetic or electric parts feeding the other, depending on polarization direction.

Rupturing the band gap: In the have topological insulators, or semiconductors the carriers transmit through specialized paths, the valence and conduction bands do not remain flat mostly separated by an energy gap, they bend to touch each other. These are called broken bands, where the fermi surfaces of the valence and the conduction band are curved so much that they are ruptured (Figure 8.3c). The critically curved regions may extend valence to conductance bands, even make contacts (Dirac points). These contact paths are topological routes, a carefully crafted path on the materials through which the changes move, or simply send phase information without any physical communication. Such points are called avoided crossing. Multiple paths are shown as capacitor like gaps in the broken band. For tunneling probability of being zero in the avoided crossing, $P = \exp(-2\pi^2/4\psi) = 0$, or $\psi = 0$. In a crossed parallel pathway, the trapped charge, does not come from anywhere,

whatever few available already there, reflect back and forth between E_{F1} and E_{F2} , with an energy gap Δ . During repeated reflections, a charge remains occupied, one could use an occupation function used by Esaki and Tsu in their historical work in the 1980s,

$$N(P_z) = \ln \left[\frac{1 + \exp((E_{F1} - E_{F2})/kT)}{1 + \exp((E_{F1} - E_{F2} - \Delta)/kT)} \right] \quad (8.3)$$

8.2 FUNDAMENTAL STRUCTURAL PARAMETERS OF A FOURTH-CIRCUIT ELEMENT—HINDUCTOR

Most magnetic field studies are performed by applying the field externally, here we are arguing that there is a possibility to generate the magnetic field naturally, in a non-magnetic material. Shaping the field using a quantum antenna is gaining interest as tiny antennas need to be arranged in a geometry that looks like a superposition of wave functions. At resonance, the product of the wave functions of tiny antenna systems generates a path made

of singularity points in the phase space. This is similar to a quantum system where we take the product of wave functions, not sum to represent a system. Functional groups in a spiral array could act like a quantum antenna that reshapes the electromagnetic wave input into a torus like a packet of magnetic flux and explore how multiple antennas to be placed in a 3D space so that their quantum coherence does not de-phase. There are three key factors in the design of a fourth-circuit element, H (Figure 8.4a–e). First, the barrier heights of a quantum well depend on the quantity of stored charge. If the height is increased, a trapped wave has to reflect many more times between the walls before leaking through. It is like adding a greater number of turns in a coil increasing the magnetic flux. Second, to squeeze the density of states of a quantum well within a narrow gap, the barriers have different resonance frequencies around the Fermi level of the well. As an electromagnetic wave passes through a high-density region, it converts a part of its electric field to the magnetic field so the emission is magnetic in nature (electromagnetic lensing). Third, without wiring physically, we place all quantum antennas in a 3D space on the path where emission from a single well experiences a singularity at resonance. It enables an array of a quantum antenna

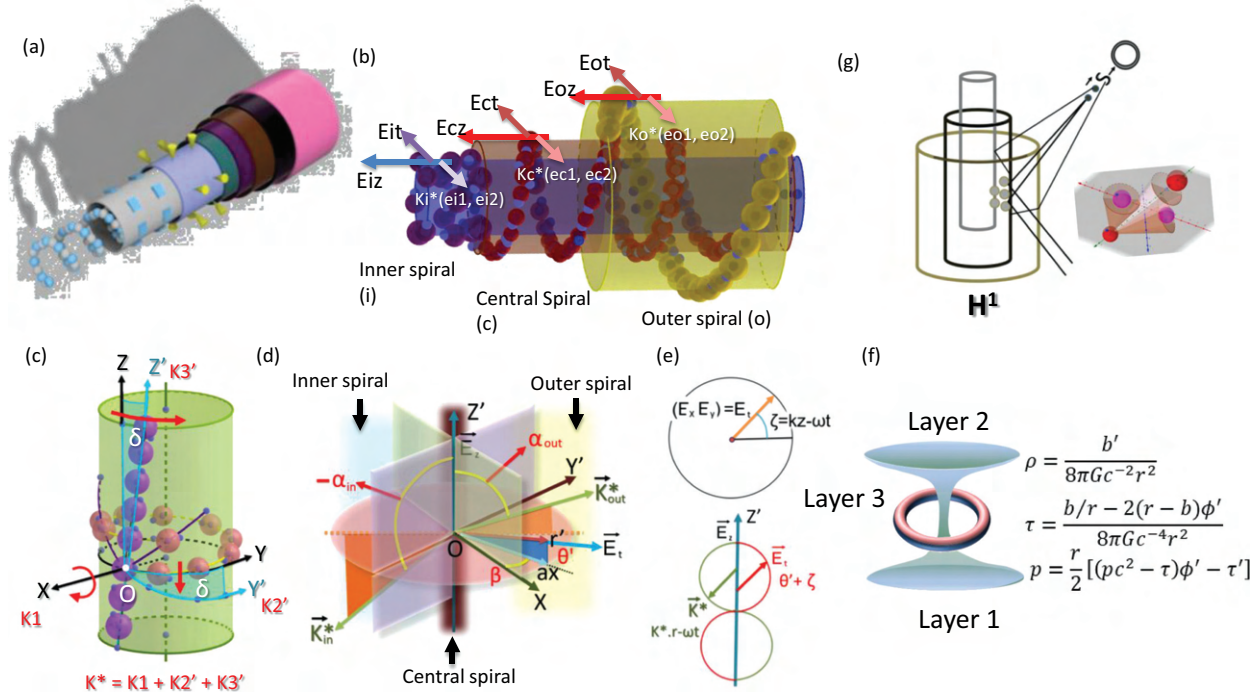


FIGURE 8.4 (a) The commercial prototype of an H device. A spiral is connected to an array of antenna and charge flux measurement probe. (b) The basic device structure with three concentric spiral layers. (c) Twisting of the spiral, a fundamental requirement to build edge and screw dislocations as the one DNA or microtubule have. (d) The cross-section of the device shown in panel b, three spirals are invisible for clarity and we have put the vectors oriented at different directions. (e) The transverse electric vector E_i is shown that the device has to neutralize to get pure magnetic vortices (top), the effective neutralization vector k^* acts to neutralize E_i . (f) The ring of fields produced at the interfaces, i.e. between two layers, these rings or lines formed by interference could move like a particle. (g) Magnetic lines or rings produced at the junction between two layers could travel like optical vortices as shown here using a schematic.

to produce a phase space identical to a single antenna. Asymmetric quantum well means its barriers have different resonance levels, so, if the gap is reduced, the density of states of the well is squeezed, the input electromagnetic wave experiences a lensing effect. When the wave function of the well's density of states oscillates periodically, the absorption of an external electromagnetic signal leads to a rapid oscillation and emission of a coherent burst. Therein, lensing ensures that the transverse component of the electric field contributes to the magnetic field. Consequently, in the emitted wave, the magnetic vector dominates over the electric vector. If we insert one such an asymmetric well inside another, since, two squeezed levels act as the walls of a non-physical quantum well, the lensing and the noise filtering abilities increase manifold. The heights of the walls not only quantify the charge content but also determine the number of times the rapidly oscillating waveform would reflect between the walls before leaking through or emission.

How does the necessity to survive under noise leads to the nested capacitor and nested inductor: a precursor to a fractal network of resonators: Students are often ask “why is it difficult to take out an electron from a solid?” The teacher replies that an electron becomes a property of the entire solid. Taking it out means snatching it alone from all the neighboring atoms that make the solid. Similarly, when the wave packets nest, the noise has to break the nesting, and dephasing a single wave won't work. Thus, the nesting of waves does not have to be a quantum one, it could be a classical nesting of waveforms. Fourth-circuit element avoids dephasing not by silencing the noise, but by packing the phase of the constituent waveforms fractally while arresting the electron flow critically—super non-conductivity could a new route to scale free integration of wave functions under noise. The idea to arrest the waveforms by manipulating a materials reflectance and transmittance came in the 1980s when the concept of quantum capacitance (Luryi, 1988; Brown et al., 1989; Ilani et al., 2006) and quantum inductance (Liu, 1991; Begliarbekov et al., 2011; Asakawa, 2010; Wang et al., 2007) came into being. The concept of reflectance and transmittance is very classical. Imagine there is a capacitor. Inside that capacitor there is another pair of electrodes. Now the bigger host capacitor would lose a part of the transmitting wave to the small capacitor. Some of the waves would get trapped by creating a capacitor inside a capacitor. It could even be possible that when the waves get trapped in the guest capacitor, a part of it leaks. The leaked wave would be out of phase than the input wave to the guest. so the out of phase wave would be representing an inductor. Now, these nested capacitors and inductors would be a quantum device if the trapped energy levels are so closely spaced that the uncertainty in energy comes into effect. Quantum or not, nesting of capacitors and inductors make sure that there is a nesting of electronic resonators, and the cleverly designed array of resonant tunneling diodes could turn the medium into a super-super-insulator, by trap inside a trap inside a trap....

8.2.1 PERIODICALLY OSCILLATING EDGE AND SCREW DISLOCATIONS

Figure 8.4b describes three concentric coils, which is a fourth-circuit element. We take one of the coils in Figure 8.4c. If we twist the coil, we get a screw ($\delta = 0$; $\delta = \pi$; left-handed and right-handed, respectively) and edge ($\delta = \pi/2$) dislocations of zig-zag paths on the coil surface. Since the coils are twisted, a mixed screw and edge dislocations on the YZ plane of coil surface rotates the X-axis by an angle δ , so that the YZ plane turns after rotation by an angle δ , a precision is given by an angle \emptyset

$$\left. \begin{aligned} r(x, y, z) &\rightarrow r'(x, y', z'); k(k_1, k_2, k_3) \rightarrow k^*(k_1, k_2, k'_3); \\ s(k^* \cdot r - \omega t) &\rightarrow s + \Delta(k^* \cdot r - \omega t + \emptyset); \zeta = kz - \omega t \end{aligned} \right\}$$

The process is explained in Figure 8.4d. Imagine that we are looking from the side of a three-concentric spiral system. In Figure 8.4d, OZ' is the central spiral, how the vectors orient with respect to the inner and outer coils are shown, the top view is schematically presented in Figure 8.4e. The amplified electromagnetic, em signal ($B \ggg E$) is perturbed by two dislocations generated signals, $e_1(e_1 e^{i(s)})$ and $e_2(e_2 e^{i(s+\emptyset)})$, interferes and creates dark lines $\Psi_n(r, t)$ made with pure magnetic fields ($E = 0$) and electric fields ($B = 0$). For magnetic lines, the real parts of $E_t = (E_x, E_y) = 0$, but the polarization $\Delta e = e_1 - e_2$ governs the knot shape shown in Figure 8.4f.

$$E_x = \operatorname{Re} \left\{ kr'e^{i(\theta'+\zeta)} + e_1 e^{i(s)} \right\} = 0 \quad (8.4)$$

$$E_y = \operatorname{Re} \left\{ ikr'e^{i(\theta'+\zeta)} + ie_2 e^{i(s+\emptyset)} \right\} = 0 \quad (8.5)$$

By equating the coefficients we get the dark spiral knots with the radius $\Delta e / k$, pitch

$$\Delta z' = \frac{\lambda \sec \delta}{2} \begin{cases} < 0 & \text{right-handed} \\ > 0 & \text{left-handed} \end{cases} \quad (8.6)$$

and the velocity $v = c \sec \delta$, we find s, θ' , i.e., locations of pixels on the pure 3D magnetic lines ($E = 0$), where, the path for dark line is given by

$$D(s, \theta') = kr' \cos(\theta' + \zeta) + e_1 \cos(s) = 0 \quad (8.7)$$

At $\infty < 0$, the inner spiral generated knots perturb the central coil knots; at $\infty > 0$, the outer coil knots perturb the central coil knots. If the inner and outer coils are pumped with even 0.1 dB GHz noise, a very low 0.1 dB input signal

$\hbar\omega$ generates a high intensity of B lines. Since three layers are identical, G-mode frequencies are very close, it triggers beating, B knots get sharper. How electromagnetic wave falls on the surface and creates interference is shown in Figure 8.4g.

8.2.2 TOPOLOGY REGULATING THE POLARIZATION

The B knots or magnetic free particle-like fields are output of two interactions, internal clock and perturbation clock (Figure 8.5a). The top cylindrical surface is a crystalline dielectric, conventionally the Pancharatnam-Berry phase of the electronic Bloch wavefunction represents the polarization (Resta, 1997). Here, the magnetic vectors interfere with creating vortex atoms, or artificial structures, they hold nested Hilbert space or polarization tensors in the 11D space. There is no electron flow, no hysteresis. A light with an electric vector rotating around the propagation axis develops an angular momentum, it is possible to change the

direction of rotation and thus execute phase transition. Many years of research has led to a situation now, where, if the rotating light rotates again in a loop path, it is possible that multiple isolated loops interact and changes rotational direction, i.e., breaks polarization symmetry (Copie et al., 2019). Fresnel refraction from surface reflect charge distribution, Figure 8.5b shows charge distribution and optical reflection side by side.

Production of coherent and polarized signal from noise: a saga of twisted spirals: Noise to polarized light conversion is known (Heebner et al., 2000). Cylindrical spiral is a crystal, the diffracted electromagnetic signal does not originate from high electron density surface plasmons, but an incredibly strong insulator. Electrons cannot move from one site to another; they absorb noise depending on the cell configuration, but the energy they emit is quantized, thus monochromatic, or singular frequency. Most importantly, since spirals are twisted, similar to thermal noise birefringence (Reuter et al., 2012), the twist leads to an edge-screw defect that creates a pair of plane-polarized signals from the cellular

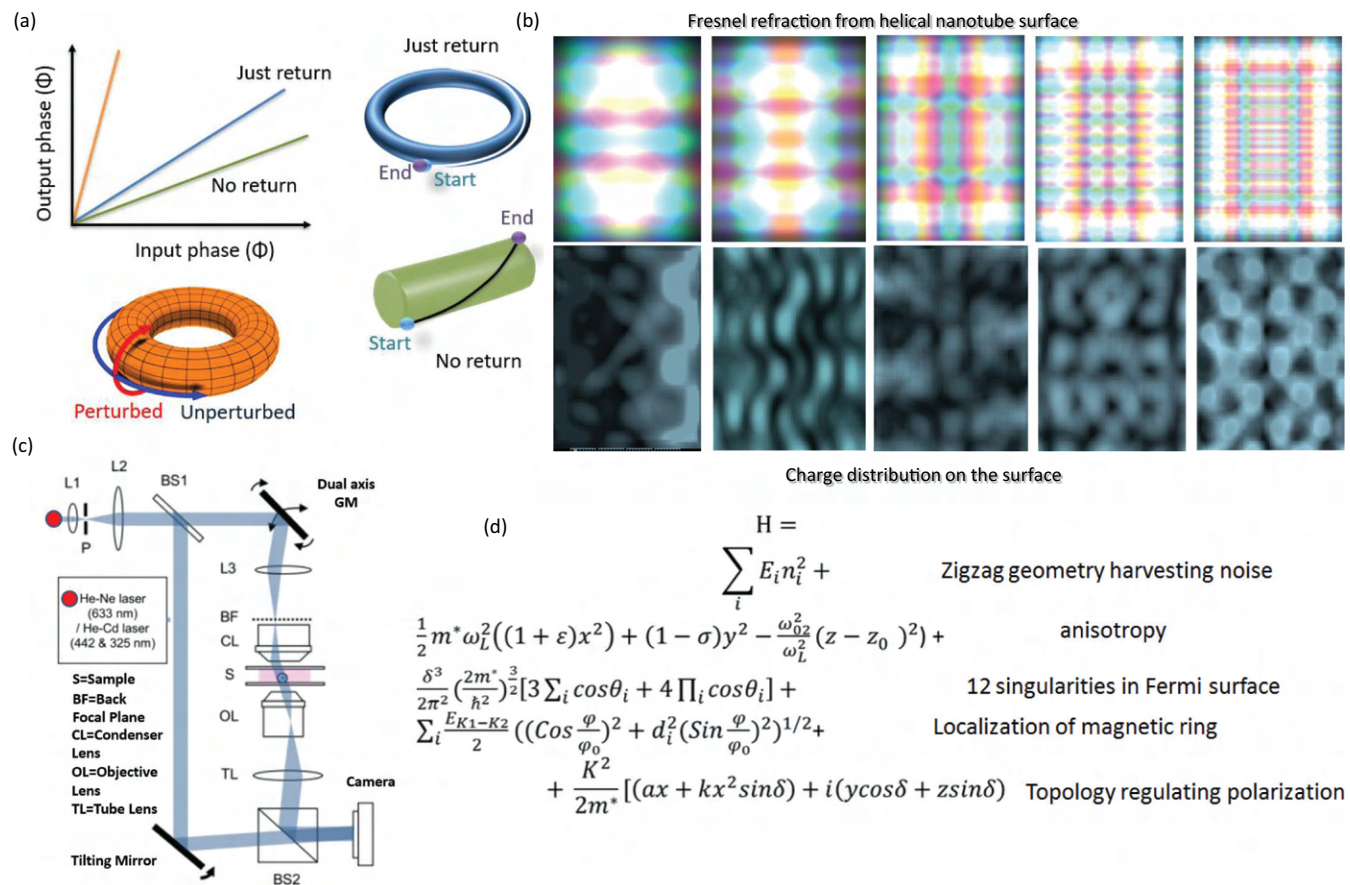


FIGURE 8.5 (a) In a periodically oscillating system, if a clock is disturbed it would change and return. The return path is traced using a cylinder and an important parameter is checked whether both the original clock and perturbed clock reach same time. Three-cylinder represents three plots for three possibilities. (b) Fresnels diffraction patterns on the microtubule nanowire surface (top), and the corresponding distribution of charge density on the surface measured for 8–25 MHz electromagnetic frequency pumping to the device. (c) Optical measurement set up for observing the optical and magnetic vortex. (d) Different parts of the Hamiltonian. Fresnel diffraction patterns, which are the shadows cast by small apertures when using a plane source of monochromatic light as a light source. <http://www.falstad.com/diffraction/> <http://www.falstad.com/modebox/>

emission. Consequently, conversion of noise to a plane polarized monochromatic signal by a material similar to an interferometer (Figure 8.5c) is a key here. We add inner and outer coils to a central coil to perturb each other, interfere and generate the dark lines. The interference between the central coil and the inner coil is very different from the interference between the central coil and the outer coil, since perturbation angle α is negative and positive, respectively (Figure 8.4g). Each of the two distinct interference events is from the superposition of four coherent sources.

8.3 THE HAMILTONIAN OR ENERGY OF FOUR CLOCKS CREATING MAGNETIC LIGHT

Figure 8.5d describes the Hamiltonian that gives energy for this device has five parts $\mathbf{H} = \mathbf{H}_1 + \mathbf{H}_2 + \mathbf{H}_3 + \mathbf{H}_4$. The Hamiltonian is plotted in Figure 8.6a. If a pair of crossing paths have n_i number of clocking waves $\vec{\psi}_{Osci}$, each wave with an energy E_i , then total energy filtered from noise is $\mathbf{H}_1 = \sum_i E_i n_i^2$. The zig-zag path filters noise in a strictly quantized manner, the separated energy of clocking wave is $\Delta\epsilon_{\pm} = \hbar k_F^2 / 2m^* = \pm\sqrt{2(1-\cos k)}$, which is part of the total energy hold by a pair of zigzag paths K_1 and K_2 , is

$$\mathbf{H}_2 = \sum_i \frac{E_{K1-K2}}{2} \left[\left(\cos \frac{\varphi}{\varphi_0} \right)^2 + d_i^2 \left(\sin \frac{\varphi}{\varphi_0} \right)^2 \right]^{1/2}$$

Here, φ is the exchanged quantized flux between the paths (flux degeneracy) with respect to a flux minimum φ_0 and d_i separates two parallel paths, k is the wave vector. The charge asymmetry between the paths holds an energy

$$\mathbf{H}_1 = \frac{1}{2} m^* \omega_L^2 \left(((1+\chi)x^2) + (1-\sigma)y^2 - \frac{\omega_{02}^2}{\omega_L^2} z^2 \right),$$

where χ is anisotropy factor, here conductivity σ distinguishes the diffracted waves ω_{02}, ω_L from different paths and layers respectively. Reflected monochromatic light interferes, the geometric parameters L, P, D , and ab regulate the strength of magnetic flux and geometry of magnetic vortices. It is $\mathbf{H}_3 = \frac{\Omega^3}{4\pi^2} (2m^*/\hbar^2)^{\frac{3}{2}} [3\sum_i \cos\theta_i + 4\prod_i \cos\theta_i]$. If we twist the coil, we get a screw ($\delta = 0; \delta = \pi$, left- and right-handed, respectively) and edge ($\delta = \pi/2$) dislocations of zig-zag paths on the coil surface the energy of the dark lines ($E = 0$) is given by $\mathbf{H}_4 = k^2/2m^* [(ax + kx^2 \sin\delta) + i(y \cos\delta + z \sin\delta)]$.

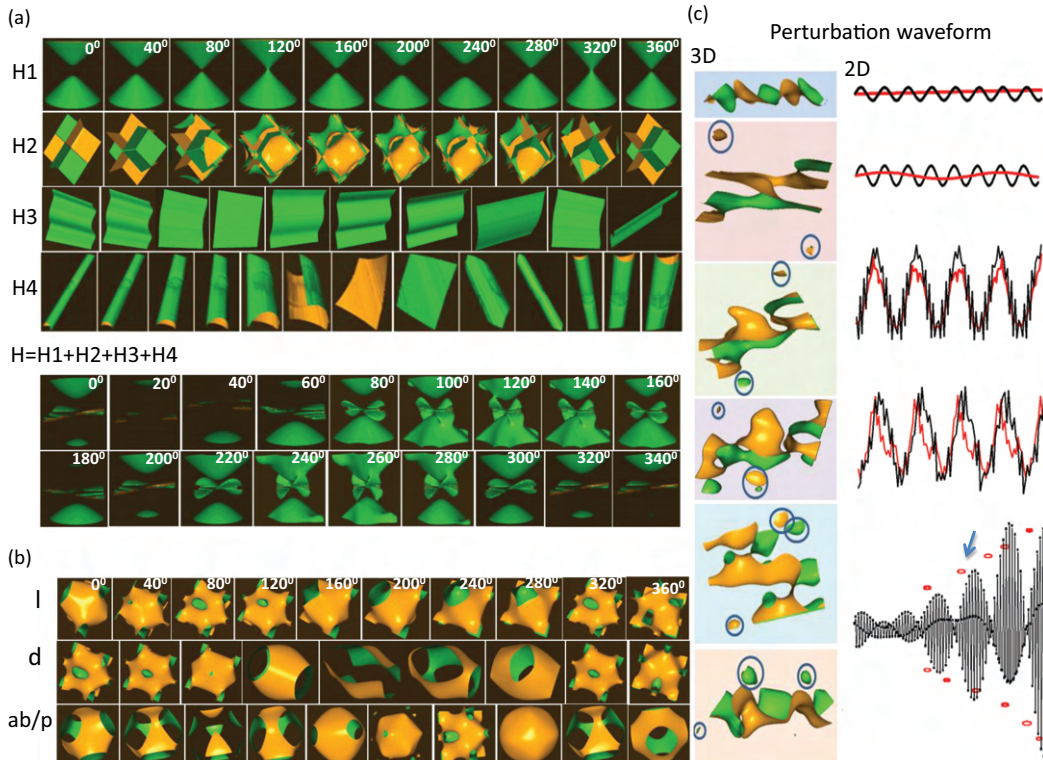


FIGURE 8.6 The four Hamiltonian parts of the generic Hamiltonian that represent the H device is shown, the value of the Hamiltonian is plotted against the variables concerned in those typical Hamiltonian. 0–360 phase change for the periodically oscillating parameter shows distinct features (top). The combined Hamiltonian shows unique behavior very different from all. (b) H2 shows a brilliant function that is fundamental to H device, sum of cosines and product of cosines. By changing length l, diameter d and the ratio of lattice area ab and pitch p, periodically the number of singularities in the phase space is tuned, shown in a series of plots as a function of phase. (c) The effective dark line formed by the interaction of multi-layered helical cylinder generated magnetic dark knots are shown where polarization and average amplitude of perturbation signals are changed.

The part $(ax + kx^2 \sin \delta) + i(y \cos \delta + z \sin \delta)$ is solved by simplifying the defect on the coil surface, considering that a dark line is $\psi = k(ax + iy')e^{i(kz - \omega t)}$. Numerical solution of \mathbf{H} for generating dynamic magnetic vortices is easy to generate. Here, \mathbf{H} forms a broken band-like structure with two-cone facing each other. Periodically, as a function of time, two new cones are born at the top cone edge, extend below, touch bottom cone edge, then slowly disappear. Then a similar thing happens at the bottom cone; together we call it conical blinking.

Including all factors here we find the Hamiltonian \mathbf{H} of the device

$$\begin{aligned} \mathbf{H} = & \mathbf{H1} \left\{ \sum_i E_i n_i^2 + \frac{1}{2} m^* \omega_L^2 \left(\begin{array}{c} (1+\varepsilon)x^2 + (1-\mu)y^2 \\ -\frac{\omega_{0i}^2}{\omega_{Li}^2} (z - \cos \phi)^2 \end{array} \right) \right\} \\ & + \mathbf{H2} \sum_i \frac{E_{K1-K2}}{2} \left\{ \begin{array}{c} \left(\left(\cos \frac{\varphi}{\varphi_0} \right)^2 + d_i^2 \left(\sin \frac{\varphi}{\varphi_0} \right)^2 \right)^{\frac{1}{2}} \\ \alpha(x_1 x_2 + x_3 x_4) \\ + \beta(x_1 x_3 + x_2 x_4) \\ + \gamma(x_1 x_4 + x_3 x_2) \end{array} \right\} \\ & + \mathbf{H3} \frac{\Omega^3}{4\pi^2} \left(\frac{2m^*}{\hbar^2} \right)^{\frac{3}{2}} [3 \sum_i \cos \theta_i + 4 \prod_i \cos \theta_i] \\ & + \mathbf{H4} \frac{K^2}{2m^*} [(ax + kx^2 \sin \delta) + i(y \cos \delta + z \sin \delta)] \end{aligned} \quad (8.8)$$

The function is plotted in Figure 8.6c. One could notice the formation of the magnetic vortex-like magnetic rings (bottom, arrow Figure 8.6c).

Coupling Coefficients CC_i are α, β, γ , and x_{1-4} is reflection coefficient $S11$ from the dielectric resonator of the four corners of cell i forming the lattice unit. $CC_i = (\alpha(x_1 x_2 + x_3 x_4) + \beta(x_1 x_3 + x_2 x_4) + \gamma(x_1 x_4 + x_3 x_2))$ When geometric parameters change as a function of time, all four parts of Hamiltonian looks different. Here we show how to change $\mathbf{H3}$.

$$\begin{aligned} \Gamma_i(r) \rightarrow & [3 \sum_i \cos \theta_i + 4 \prod_i \cos \theta_i] \rightarrow \Gamma_i(r, t) \\ = & 3 \sum_i \cos(x_i \cos t_i) + 4 \prod_i \cos(x_i \cos t_i) \end{aligned} \quad (8.9)$$

The function is plotted in Figure 8.6b.

8.3.1 BIREFRINGENCE, QUANTUM BEATING AND CLASSICAL BEATING

The development of the fourth-circuit element requires a few fundamental materials properties, as outlined in Figure 8.7a. The following describes them one by one.

Birefringence and metamaterial: Optically or electromagnetically operating quantum devices can process quantum states at room temperature and in ambient atmospheric conditions. However, it requires a pair of quantum coherent sources, for interference. Microtubule has the property of birefringence (Mithieux et al., 1985), which enables generating a pair of quantum coherent sources (O-ray and E ray; Figure 8.3a). The α -helices of a protein molecule could be considered as a single, the most elementary antenna. A protein molecule would itself be an optical antenna array, whose optical anisotropy is tailored by mechanical resonance. Such materials normally show a giant birefringence (Kats et al., 2012). Such a surface controls the polarization of the reflected light (Zhao and Alu, 2011). The reflected wave from the protein made microtubule surface interferes and forms geometric structures made of dark lines where, due to destructive interference, there is no light. The structures of darkness produced by microtubule or its analog Hinductor devices do not remain static due to the water crystal of microtubule, it perturbs, and the knots of darkness rapidly changes the shape with time, periodically. Inner water, tubulin protein, and outer water of microtubule make three concentric layers required for building a fourth-circuit element (Figure 8.4). So, we get clocking geometric shapes like a time crystal. In these dark lines $E = 0, B$ is not zero, i.e., these are magnetic structures. The dark structure-made geometric shape is a function of charge distribution on the microtubule or H surface. It is a well-established theory that the reflection property depends on the charge distribution of a surface. Now, by applying a noise bias, we can tune electron density and the magnetic structures. It naturally creates clocking geometric shapes, and could store time crystals for a long, long time powered by noise. Simply by soldering capacitors in series and rolling them along a spiral one could test the linearity of magnetic flux and charge. Artificial structures analogous to microtubule show a distribution of magnetic flux as a function of heat flow on its surface (Figure 8.7b). The linear magnetic flux vs charge stored in the capacitors by applying noisy pulse suggests that (Figure 8.7c), charge flow may not be required at nanoscale too. Figure 8.7d shows a magnetic flux hysteresis for a single microtubule. These experiments prompted us to do more complex experiments on capacitor analog, that is not a true device, but, easy to check basic ideas.

Interference of four sources in intimately coupled coils: **A path to geometric musical language (GML):** Negative refractive index of a material is fundamental to the emergence of metamaterial, because for a material to be a metamaterial the signs of magnetic permeability and dielectric permittivity should have to be reversed (Shelby et al., 2001; Valentine et al., 2008; Yu et al., 2011). We noted above that each coil generates a pair of coherent signals due to birefringence like events, and we get circular or elliptically polarized signals. However, three coils are connected; the separation between them is that of atomic bonds. Thus, three coils act like single molecular architecture. Hence the noise converted into a pair of coherent signals in the central coil bifurcates into the inner coil and the outer coil. Then two independent interference

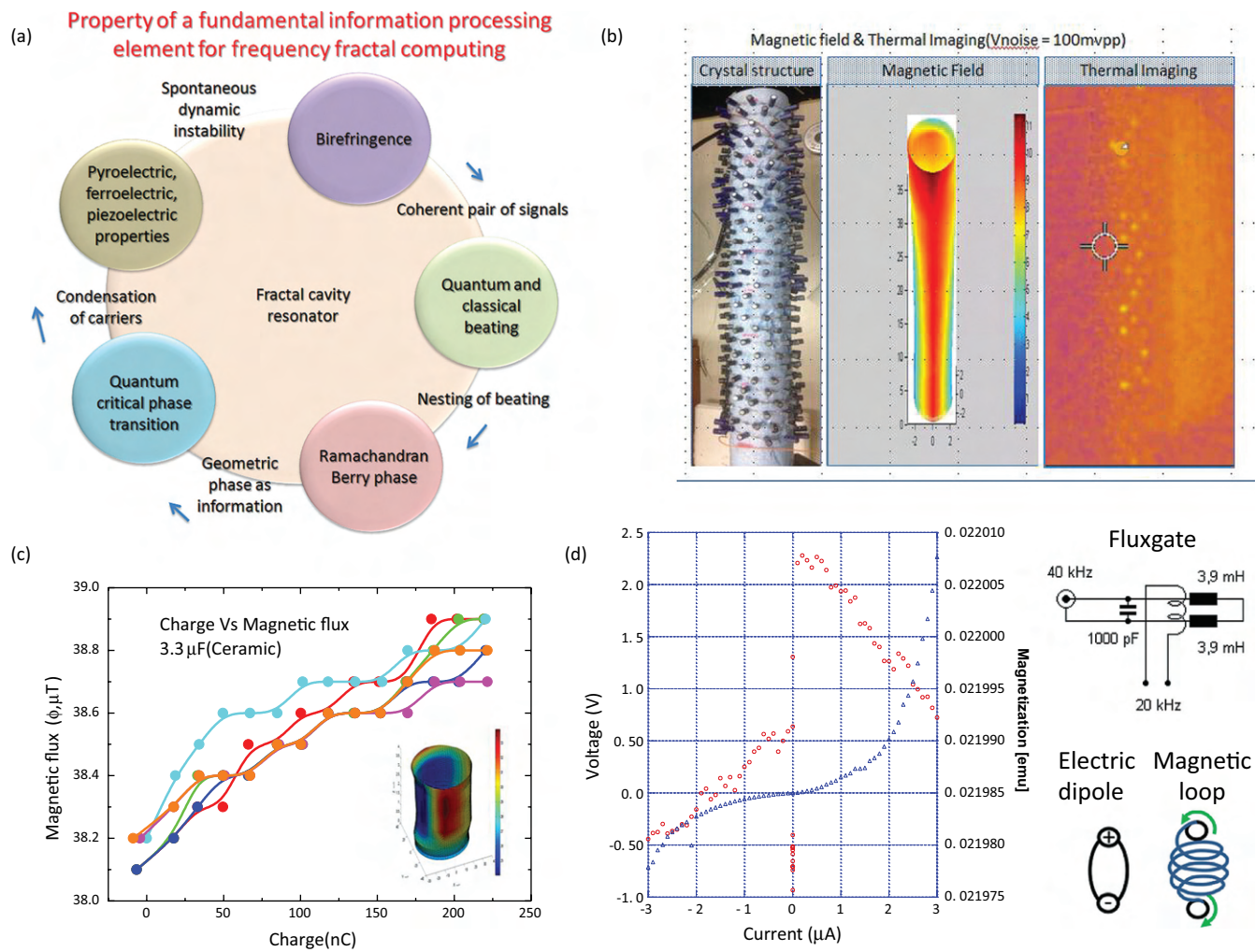


FIGURE 8.7 (a) Physical phenomena that operates a fourth-circuit element device H. (b) A simple demonstration of H device (left) by pumping electromagnetic noise MHz-GHz range to the device and measuring the magnetic flux produced on the surface of arrayed capacitors (10s of microfarads), middle, and to the extreme right, thermal images show that heat exchanges between the capacitors. (c) The charge stored on the surface of the device and the magnetic flux produced was measured for different helical coils made of different capacitances. (d) Using picotesla sensitive fluxgate magnetometer magnetization of single microtubule is measured.

events happen. One interference of four waves occur between the inner and central coil; the other interference of four waves occurs between the central and the outer coil.

$$\begin{aligned}\Gamma &= \Gamma_1 + \Gamma_2 + \Gamma_3 + \Gamma_4 \\ &= 4\sin(kz - \omega t)\cos(\pi ds\sin\theta/\lambda)\cos(2\pi ds\sin\theta/\lambda) \\ &\sim \cos\rho_1\cos\rho_2\cos(\rho_3\sin\theta)\end{aligned}$$

Due to a common wall between the coils, a coherence between the bifurcated sources are ensured.

The basic requirement of GML is a clock. If three plane waves interfere, we get a straight line, if four plane waves interfere, the vortices rotate like a clock Ψ (O'Holleran et al., 2006). If five waves interfere, we get an irregular pattern. Each clock Ψ holds a singularity point. Note that the geometric shapes

are inequality relationship hold by the clocks. For example, $\Psi_1 + \Psi_2 \geq \Psi_3 \dots$ triangle. $\Psi_1 + \Psi_2 + \Psi_3 \geq \Psi_4 \dots$ quadrilateral. $\Psi_1 + \Psi_2 + \Psi_3 + \Psi_4 \geq \Psi_5 \dots$ pentagon. Different composition of cross-bar pathways on the Hinductor coil forms magnetic rings of different diameters representing $\Psi_1, \Psi_2, \Psi_3 \dots$. These distinct rings could interact to integrate into a higher-level clock.

8.3.2 PANCHARATNAM BERRY PHASE

As described in Chapter 4, the concept of geometric phase is easy to conceive if we consider microcoil or nano coil resonators and shine it with polarized light (Lee et al., 2011). Since Hinductor is all about multilayer concentric columns, adding geometric phase is easy. If noise is pumped along the column of a spiral, the dominating magnetic flux morphs a ring. If the noise is pumped on its surface ($\sim 23^\circ$ for microtubule), the flux adopts a spiral shape. At resonance, as the

phase changes 0° – 360° , both the ring and the spiral shape oscillate with noise. If the noise intensity V is within limits ($20 < V < 80$ mV), ~500 times below the charging bias of a capacitor and the frequency bandwidth of noise could hold $g_{v(r)}$ number of resonance peaks, then the local magnetic wave degeneracy is $g_v = g_{v(r)} \times g_{v(a,b)}$. Sahu et al. imaged a pair of THz magnetic wave observed in a rectangular and in a hexagonal lattice, but no current or field flow was observed. Topology change rearranges the fields whose vector sum is zero. Accumulation of magnetic flux is not from more current flow by amperes law, but the adjustment of shined light on the electron density surface.

The magnetic waves generated by splitting of noise interfere due to the helical period experienced by a lattice (a, b). The magnetic field could tune quantum beating (Henke et al., 1981) in the microtubule and in its analog H device ($\emptyset \sim g_{v(ab)} e^{i\theta}$). As the frequency gap between the coherent sources is low, a THz noise beats at GHz frequencies surviving around a pair of lattice units. These GHz oscillations interfere again ($\theta \sim g_v e^{i\alpha}$) due to length, pitch, and diameter constraints, beat at MHz ($f_0 = \Delta f = 0.0000001$ THz ~ 1 MHz), surviving around thousands of lattice units. The condensed magnetic wave ($\emptyset \sim g_{v(ab)} e^{i g_v e^{i\alpha}}$) is imaged live, two-level magnetic interference integrates a local lattice to its global topology. Waves couple classically by adding/subtracting phase, quantum phases couple as a product, but here, in the beating of beats, the phases couple exponentially. A pair of microtubules synchronously beats at multiple time scales at a time, due to the beating of beats. The difference in frequency of participating waves is the beating frequency of a new wave, but that wave could undergo beating once again.

8.3.3 PYROELECTRIC, FERROELECTRIC, AND PIEZOELECTRIC PROPERTIES

Biological materials are often depicted as ferroelectric and piezoelectric since under a mechanical pressure they release ions as current flow, and at a suitable electric bias desorb/absorb ion reversibly. A true ferroelectric material should have an intimate correlation between the applied bias and its dipolar orientations, flowing current under pressure and reversible conductance switching are not sufficient. Bandyopadhyay et al. have imaged live the resonant oscillations of DNA, RNA, proteins like actin and their complexes via tunneling current, which show that unlike inorganic materials, these are soft like a liquid drop. The concept of “lattice-like ordering of dipoles” or even a “domain of unidirectional dipoles” does not exist therein. Porcine brain neuron-extracted tubulin has 8 tryptophan and 36 tyrosine residues (Ponstingl et al., 1982), and as the temperature increases, a smaller number of tryptophan residues are exposed. Denaturalization via unfolding has two linear domains, first 20°C – 40°C and second, 55°C – 90°C , in these regions, a conformational change is homogeneous (Mozo-Villarias et al., 1991). The interesting transition at 40°C – 55°C is caused by the conversion of just one tryptophan residue from exposed to the unexposed configuration.

Since this transition stops reversible switching of the tubulin charge center by 1.2\AA , dipolar switching by $\pm 23^\circ$ is blocked, and tubulin is left with only one energy minima, tubulin switches from two energy minima to one; therefore, microtubules Curie point should be located here. In the 20°C – 40°C domain, both tryptophan and tyrosine residues change conformation and unfold in the same rate; however, in the 55°C – 90°C region, tryptophan residues denaturize faster than tyrosine residues, and at $>55^\circ\text{C}$, less than 4 tryptophans remain exposed, at 90° , tubulin is permanently denaturized (Audenaert et al., 1989). The scanning tunneling microscope (STM) images of multiple structural phases of single tubulin dimer; these transitions were artificially induced in the structure in a controlled manner.

Similarly, a structural phase transition occurs in the microtubule lattices as observed in the cryo-TEM where rectangular to hexagonal lattice transition is visible in the microtubules in the neuron (Kikkawa et al., 1994). Porcine tubulins assemble into microtubule via distorted hexagonal close packing with a unique polar direction which assigns lattice-type A to enantiomeric polar crystal class (point group C_6) and lattice-type B pure polar class (point group C_{6v}). Both the lattices favor a spontaneous pyroelectric and ferroelectric effect (Wu et al., 2009; Bruce et al., 2011), notably, out of 32, only 10 polar crystal classes favor these effects.

Effective electronic polarization co-efficient or the ionic polarizability α normalized for microtubule length is $6.3 \pm 0.3 \times 10^{-24}$ cm (Minoura and Muto, 2006; microtubule has 10% of the value of BaTiO_3), charge density is 20 e/dimer, 2.5 e/nm along one protofilament, hence 32 e/nm in a 13 protofilament microtubule. Hence, polarization measurement should start after all these charges are released; otherwise, we see clockwise current-voltage characteristic. For a true ferroelectric, polarization in hysteresis is counter-clockwise. A single microtubule's perfectly square or lossless hysteretic current-voltage (IV) characteristic at 10^{-6} Torr and in ambient conditions depicts a ferroelectric behavior, since remnant polarization P_{rem} sends leakage current at zero bias; red arrow denotes threshold switching voltage. Microtubule showed $P_{\text{rem}} \sim 3 \text{ C/cm}^2$, which is 10^6 times more than normal ferroelectrics; however, it is feasible since microtubule charge density $10^{20}/\text{cm}^3$ is orders higher than normal insulator ferroelectrics. For P_{rem} coercive field is 0.6 kV/cm. Similar to a classical ferroelectric, microtubule holds the charge ($\Delta C/C$) until Curie temperature, and dielectric loss measurement supports the inherent dipolar transition.

8.4 LINEAR VARIATION OF MAGNETIC FLUX AND STORED CHARGE IN H

Derivation of H between the stored charge Q and the magnetic flux Ψ : Group of stored charge Q diffused by noise combines the lattice spin waves (a and b are lattice parameters), by addition (like classical) and product (like in quantum) of phase $z = (\sum z_i + \prod z_i)$ as they beat locally ($z = e^{i\theta}$). Due to global topological constraint spread over three directions

(diameter, D; pitch P; length L) local waves interfere with beating frequency generated signal.

We get for the beating of beats $e^{\delta^3 z} = e^{\delta^3(\Sigma z_i + \Pi z_i)} = e^{\delta^3(3(z_D^\dagger + z_P^\dagger + z_L^\dagger) + 4z_D^\dagger z_P^\dagger z_L^\dagger)}$.

Here, $\delta = \frac{\text{Surface area}}{\text{Lattice unit area}} = \frac{2\pi rL}{ab} = \frac{\pi DL}{ab}$. The critical parameter to integrate classical and quantum factors in phase space should be in ratio 1:1.0205, i.e., 3:3.0615. Here, 3:3.0615 is the critical point where a singularity is born. We kept quantum capacitance²⁶-induced phase factor 3:4, to keep the area of the hole created by singularity is proportional to the area covered by the phase space continuum.

The cumulative spatial phase factor of the charges $Qe^{\delta z}$ constituting the sinusoidal wave per unit velocity of photon ($Qe^{\delta^3 z}/c_m$) in that medium is the magnetic flux (since $B = E/c$, we get for entire cylindrical surface $\Psi = Qe^z/c_m = QH$).

Here, $\frac{\Psi}{Q} = H = \frac{e^{\delta^3 z}}{c_m} = \sqrt{\mu_m \epsilon_m} e^{\delta^3 z} = \frac{1}{c_m} e^{\delta^3(3(z_D^\dagger + z_P^\dagger + z_L^\dagger) + 4z_D^\dagger z_P^\dagger z_L^\dagger)}$. The nth period plays an important factor in the magnetic wave. The larger the value of n, the phase oscillation gradient increases nearly exponentially.

$$H = \frac{1}{c_m} e^{\delta^3 \left[3\cos\left(\frac{D-nb}{b}\right) + 3\cos\left(\frac{P-na}{a}\right) + 3\cos\left(\frac{L-nP}{P}\right) + 4\cos\left(\frac{D-nb}{b}\right)\cos\left(\frac{P-na}{a}\right)\cos\left(\frac{L-nP}{P}\right) \right]} \quad (8.10)$$

From magnetic rings, one could measure the total flux content Ψ by matching the ring's color intensity with a standard magnet response and plotted Ψ with Q . Both Ψ and Q varied non-linearly as a function of applied frequency $\hbar\omega$ but so similarly that the Ψ - Q plots were linear, for all materials studied, delivering a constant H , which is accurately predicted by equation (8.10). H is oscillatory as a function of L , P , and D , if the periods for a typical material are L_p , P_p , and D_p , then the periodicity index $I = L_p P_p / \pi D_p^2$. In fact, $\Gamma_i(r,t)$ explained in equation (8.9) that governs H3 and the generalized expression for Hinductance, H (equation 8.10), was discovered in >1000 devices by three independent blind studies (Karthik, K.V., Suryakant, Kumar, Pushpendra Singh) spanned over ten years. However, though the dimensions are same, H is not the resistance as its value is $\sim 10^{-4}$, while the resistance of these devices R is $\sim 10^9 \Omega$, these devices are all insulators, i.e., no current flows.

The interaction between the electromagnetic field and the quantum system is characterized by another constant, the charge, that pertains to the quantum system alone. If we look closely into the quantum analogs of classical devices, most quantum formulations do three things. First it considers that even quantum elements follow classical circuit wiring concepts, serial and parallel connections of circuit elements are only two ways to connect them. Second, it considers that a very low resistance path and low conductance fluctuation around Fermi level ($h\nu = k_B T$) is the only way to realize a quantum effect. Always, I and V are there as a common factor with Ψ or Q ; it is believed Ψ - Q pair cannot stand alone. Third, entanglement does not require a real physical communication through a well-defined path,

yet it considers a coherent real physical motion of particles within an isolated restricted barrier to avoid the dephasing. Be it a spin-wave or quantum interference, a path is always there, but never there in theory. Three legacies of classical concepts, classical wiring, resistance, and necessity of a defined path, were universally accepted in the quantum experiments and their quantum transformations were never in demand. It is utmost essential not to copy the classical treatments in quantum and also demonstrate that the effort to standalone Ψ - Q pair as independent as resistance could have a classical analog too.

Conductance, a differential of current and voltage was earlier defined as dI/dV , now as $R \rightarrow \infty$, $d\Psi/dQ \rightarrow 0$. Quantum formulations inherently consider $d\Psi/dQ = R$. It is not always true. If $d\Psi/dQ \neq R$, and undefined, then a new formulations quantum mechanics and classical mechanics are required. Since we do not supply voltage and measure current anymore, the existing formulations, all based on conductance requires a new equivalent. Similar to dI/dV , differential conductance we get $dQ/d\Psi$, while the first flow electron, the second flows phase. Since $R \rightarrow \infty$, $R = 10^{15} \Omega$ and $H = 0.001$, $dQ/d\Psi \neq dI/dV$. We need a new physical parameter. The newly invented probe that senses the differential flux-charge, only applies noise. The noise, within a limit lets the clocking continue within the well. Beyond that, the noise shortens the clocking circle's perimeter such that the electromagnetic wave turns smaller than the barrier's collision cross-section that reflects it, the wave leaks through the well barrier. Information processing in microtubule was proposed in 1982 (Hameroff and Watt, 1982) experimentally verified in 2010 (Sahu et al., 2010, 2013a, 2013b).

8.4.1 FLOW OF THERMAL WAVE—FRIEND OR FOE?

In manmade machines, friction/collision is essential to apply the torque to move a body to work, which causes the heat-loss—consequently, scientists argued a loss-less Carnot engine (Carnot and Thurston, 1890) for nearly half a century. Simply put, the target is to send energy from source to drain without any loss. Recently, the dream is explored via quantum protocols (Scully et al., 2003; del Rio et al., 2011) arguing that the quantum coherence would enable loss-less transmission and entanglement would avoid friction in a machine. Since these models keep the century-old “isolated system”—a hallmark of Kelvin's thermodynamic era, the energy-loss is inevitable when the work is translated outside. Landauer argued that the minimum energy required for one computational step in an “open system” is $k_B T$ and it could be realized using a loss-less particle-like energy-packet (Landauer, 1988) for the source-to-drain transport. Since, a Kinesin motor requires 12 $k_B T$ per step to walk through microtubule in a living cell or “non-isolated” system, the random fluctuations even by one $k_B T$ unit would cause $\sim 10\%$ error, which living cells cannot afford. Both, the engine efficiency of Kinesin cycle that varies from 0% to 100%, and the variation of growth/decay of microtubule-length with temperature have argued

microtubule as an ideal heat sink (Caplow et al., 1988). Since microtubule exhibits negative specific heat (Vulevic and Correia, 1997), the possibility cannot be ruled out. Moreover, the noise-induced errors are fatal to the essential vesicle transport in a living cell—alleviated if microtubule is a perfect heat sink that keeps the entropy constant even under thermal fluctuations.

The lattice mosaic of tubulin proteins on the microtubule surface works as the nesting ground for a stream of loss-less particle-like energy packets. Chemical imbalance triggers soliton in the β -sheet of protein (Kayser et al., 2004). Solitons also generate in the zig-zag chain like α -helix, microtubule surface (Christiansen et al., 1997). Helical nanowires generate solitons (Brizhika et al., 2006). Microtubule satisfies all these criteria, surface-bound states generate topological phonon modes (Prodan and Prodan, 2009). Live images are shown, how feedback management operates to balance the thermal noise and the signal collectively to keep the entropy constant between 5 and 320 K. The finding resolves the thermodynamic equilibrium debate by showing that the fluctuation in protein-entropy is the signature of feedback management to keep the entropy constant. We could not read the random-jumps in entropy, so we assigned it as noise. The Carnot engine equivalence of a single brain microtubule is derived here from direct microscopic visualization.

Dynamics of two tubulin dimers suggest that the oscillation of energy between two dimers do not stop even in the presence of a neighbor, therefore, the mechanical energy stored in the extra β -sheet of tubulin dimer cannot move alone. However, when tubulins form a nearly a ring, mechanical oscillation stabilizes. Thus, 13 tubulin dimers can disperse energy homogeneously only long the circumference of the microtubule, a concerted shift of lattice displacement is created along a circular region as a ring of energy-packets with an opening due to offset. Spiral symmetry of microtubule makes β -sheets forming spiral inside a spiral of tubulin dimers (Hunyadi et al., 2007). A helical structure naturally quantizes energy that transmits through it (Michalski and Mele, 2000). Helical structures also trigger ballistic transport (Grigorkin and Dunaevskii, 2007). The opening destabilizes the 13-tubulin ring to move longitudinally along the length of the microtubule, and nanocavities are known to generate ballistic phonon (Huang et al., 2009). This ring with an opening is a phonon-particle like energy packet, since it is visible distinctly in AFM images, but not in the STM image. Due to identical periodic paths, since creation, the relative coordinates of electronic-packets and phonon-phonon packets are automatically fixed on the microtubule surface, which locks phase and frequency of the constituent phonon- and electronic-packets locally. Thus phonon-packets move together linearly and electronic-packets move together helically as a single unit, and we call it group. Since these particle-like energy-packets are lattice kinks, they are visible in AFM if mechanical in nature and visible in STM if electronic. Filaments, in general, create a topological phonon mode (Berg et al., 2011).

The mixture of five electronic-particle groups of distinct symmetries and three phonon-particle groups of distinct periodicities appear and disappear on the microtubule surface during transport under thermal scan 5–320 K. Simultaneously, one should measure electronic-particle and phonon-particle covered area on the microtubule surface from live images. The ratio of these two areas or fraction of surface area covered by phonon-particle and electronic-particle groups is termed as the band fill factor, and the coherence reflects mutual co-operation between two kinds of particles and lattice distortions (Moskalenko et al., 1980). These deformations shrink/expand separation between protein dimers throughout the nanowire; thus, restricts the length and conductivity of the microtubule-spring (σ_E). The microtubule length, group-phase transition frequency and the rate of length change are proportional to the externally applied noise. Since, after reaching the far end, the phonon-particles are pumped out as energy, they disappear from the image, surplus/deficit of phonon-particle groups subtract/add the length of microtubule nanowire, to which electronic-particle groups respond again and return conductivity back to the initial one (σ_S to σ_E). Thus, the surface coverage of electronic-particle and phonon-particle groups is regulated in a quantized manner, and similar to a spring a feedback control returns original length and conductivity.

To calculate entropy, Sahu et al. wrote a conducting state (σ_E) at a particular temperature and by sweeping the temperature between 5 and 320 K continuously measured the conductivity. The *dc* and *ac* conductivity remains constant, except minor jumps between equally spaced values (σ_S). Even under extreme thermal noise is 1 K/minute (dQ), oscillatory flipping between two limiting conductivities is observed as temperature T changes. The entropy $S = S_0 + [d\sigma_S / T]$ plot against temperature T shows that it remains constant over time, no material is known to exhibit such feature under normal condition (Zaitsevzotov, 1993). When the entropy slips, noise is poured into the microtubule and when entropy returns it means, the noise is pumped out of microtubule. Thus, the microtubule sets a classic example of harnessing noise to keep the entropy constant; it demonstrates transport and noise-alleviation efficiency at an extreme level. The output noise current is a function of source-drain and gate bias. Here, a harmonic interference of noise propagating along the microtubule, and when there it is no noise, these are the live images of how microtubule manages noise. STM and AFM images of energy-packet transmission and interference like pattern proves that the transmitted signal across microtubule is coherent, microtubule converts incoherent signals into a coherent wave.

8.4.2 WIRELESS COMMUNICATION BETWEEN TWO H DEVICES

Magnetic coupling carries out wireless energy transfer much more easily than electromagnetic or electric coupling (Kurs et al., 2007) if there is a parity-time symmetric circuit then the power transfer is even more robust (Assawaworrarit et al., 2017).

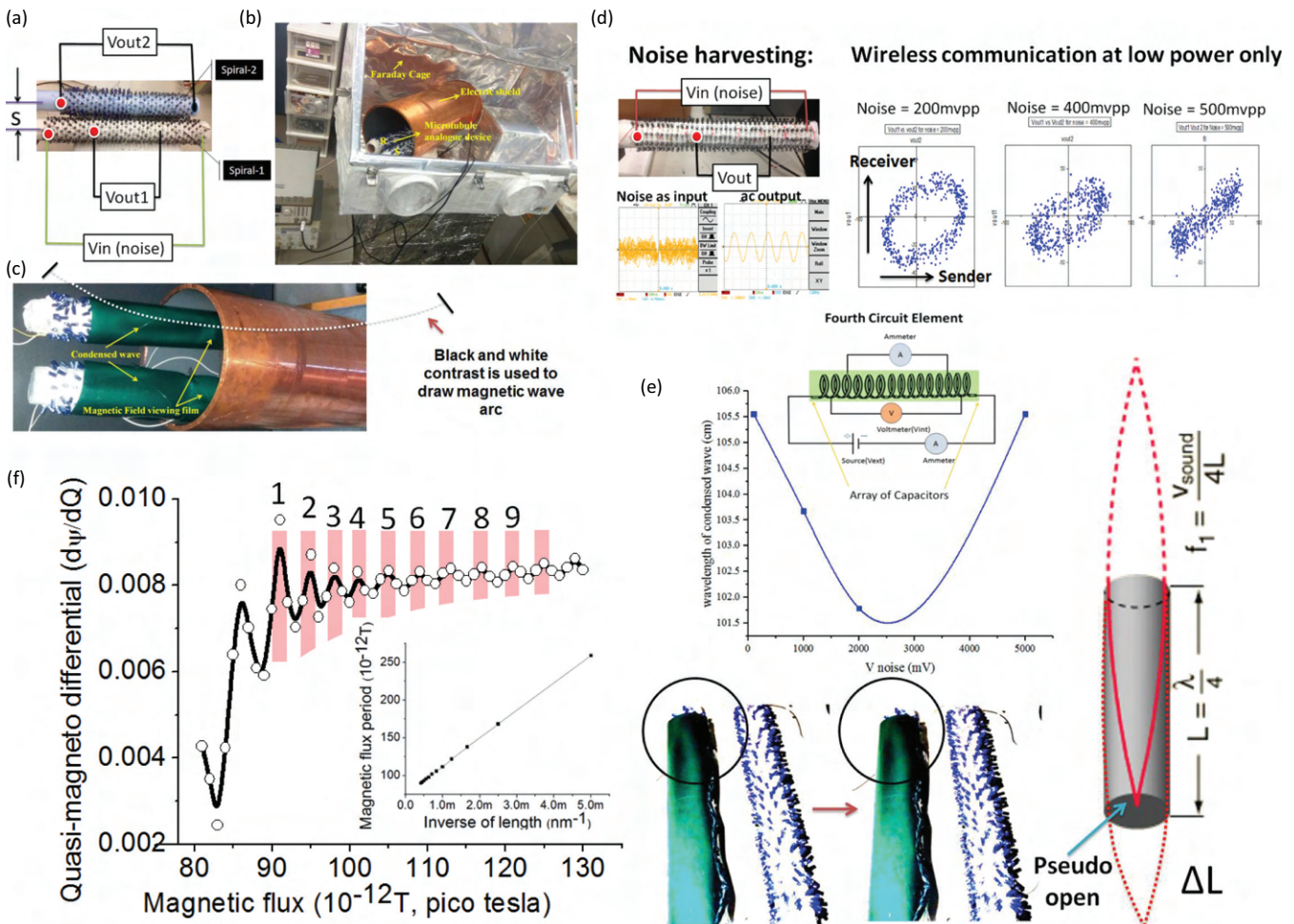


FIGURE 8.8 (a) Wireless communication between two coils, experimental setup. (b) The state of the art Faraday box, especially covered with composite materials and magnetic shields. (c) A pair of coils wrapped with magnetic films measuring the changes in the magnetic field distribution all along the surface. (d) For the coil operation continuously noise is pumped and output is an organized signal. Sender coil and the receiver coil were fed orthogonally to an oscilloscope and the phase plot shows identical energy transmission magnetically between the two coils. (e) The wavelength of the magnetic wave estimated from the coil surface for different bias. (f) Similar measurements were carried out on the surface of a microtubule. Oscillation of the magnetic flux with respect to the inverse of the flux-charge proportional constant shows periodic ripples in the values. In the inset, those ripple periods are plotted with the inverse of microtubule length. Tomasch quantum oscillations (nine ripples noted) when magnetic-charge differential measured directly by coaxial atom probe is plotted against magnetic flux. Inset is the length variation study of microtubule and finding periods of oscillations for different lengths. Inset plot was used to calculate fermi velocity of charge.

Magneto-inductive effects in the metamaterials allow even 1D data transfer (Stevens et al., 2010). Saxena et al. have carried out an extensive study on wireless communication between the pair of microtubules (Saxena et al., 2018; Figure 8.8a–c). Microtubule undergoes rapid phase changes on its surface under the exposure of electromagnetic fields of certain frequencies (Sahu et al., 2010). We can consider its surface as a composition of lattices of various lattice parameters and sizes, and all experiments are carried out by mixing noise with signal (noise>2signal; Figure 8.8b). At a particular resonance frequency, there is an equilibrium, we get $N_r^{\text{equ}} = N_0 \exp(-\Delta G_{\text{cluster}}(r)/k_B T)$, this statistically accounts the composition of lattice symmetries at resonance, where

$$\Delta G_{\text{cluster}}(r) = -\Delta G_{lc,v} \cdot \pi r^2 l_{\text{cluster}} + \sigma \pi r^2 l_{\text{microtubule}} \dots \quad (8.11)$$

Here, $\Delta G_{lc,v}$ is the energy due to a phase change per unit cluster area on the microtubule or H surface. And σ is the interfacial free energy propagating throughout the microtubule surface due to THz transmissions between tubulin proteins or equivalent capacitors.

From equation (8.11) we get $\Delta G_{\text{critical}} = 16\pi\sigma^3/3\Delta G_{lc,v}^2$ for a particular lattice configuration, i.e., greater than a critical radius, and equation (8.11) predicts a condensation above this limit. Condensation means a particular lattice starts dominating its surface. The rate of condensation of a typical symmetry in a receiver microtubule's surface is given by

$$G = S_c k N_0 \frac{1}{N_c} \left(\frac{\Delta G_c}{3\pi k_B T} \right)^{1/2} \exp\left(-\frac{\Delta G_c}{k_B T}\right) \quad (8.12)$$

Here, N_c is the number of lattice points that first synchronizes its phase in the sender with the receiver's magnetic condensed wave's phase. Now, we need to find the phase gain rate g_s from the lattice gain rate G . We explain it below.

To understand the wireless communication between the microtubule analog devices as shown in Figure 8.8d, we inherently considered the coupled-mode theory model of two resonant systems for the analysis. According to this coupled-mode theory, these two resonant systems act as a source and receiver. The source system has a resonant frequency of ω_s . The overall system gain rate is expressed as $G = g_s - \gamma_s$, where g_s is the phase gain rate of the source and γ_s is the intrinsic loss rate of the source. The receiver lattice has a resonant frequency of ω_r . The overall loss rate of the system is expressed as the $\gamma = \gamma_r + \gamma_{rl}$, where γ_r is the intrinsic loss rate of the receiver and γ_{rl} is the rate of loss at the receiver load. Power is transmitted from source to receiver with a transmission coupling coefficient rate α , which is a function of signal amplitude. Transmission coupling coefficient decreases exponentially as the separation distance between the source and receiver increases (Figure 8.8e). Here Saxena et al. supplied noise signal to the source. If V_{noise} is the noise signal and V_r is the output voltage of receiver, then the rate of change in signals is described by the following equation:

$$\frac{d}{dt} \begin{bmatrix} V_{noise} \\ V_r \end{bmatrix} = \begin{bmatrix} i\omega_s + g_s & -i\alpha \\ -i\alpha & i\omega_r - \gamma \end{bmatrix} \begin{bmatrix} V_{noise} \\ V_r \end{bmatrix}$$

8.4.3 TOMASCH OSCILLATIONS AND HARVESTING NOISE

Now, it's time to test noise on a single microtubule. We all could remember the historical journey that Tomasch oscillations or reflections in the same direction made (Tomasch, 1966; Lykken et al., 1970; Wolfram, 1968). If the path is resistance-less, then the carriers do not leave a thin, confined region, oscillates therein between the boundaries for a long time. Of course, in the initial days, finding the evidence of such trapped oscillation (Tomasch oscillation) became difficult. However, one particular point became explicit—the device geometry does play a role in the prolonged survival of a carrier in the thin confined region. Now, a long time has passed, people are trying to change from electron flow to the phase flow, and for that, the device geometry would become ever more critical (Thouless, 1998). Every clock is like a pendulum, repeatedly reflects between the two boundaries. Here, we have an unusual situation. No one would like that the network of clocks would damp. One way to resolve that problem is to vibrate the boundary of the cavity. That vibration would supply the necessary energy required to run the clock. Say, we want an electron to be trapped in a cavity and then vibrate between the boundaries for a long, long time so that it represents a clock. Differential flux charge measurement on a single microtubule shows Tomasch oscillations (Figure 8.8f).

8.5 PERIODIC OSCILLATION OF CAPACITANCE, INDUCTANCE, AND HINDUCTANCE WITH ITS GEOMETRY

Quantum resonance made of quantum inductor and quantum capacitor: Violation of Kirchhoff's law: Since the first observation of resonance by inductive and capacitive elements in 1826, whenever we observe resonance in nature, deep inside our brain to the extreme end of the galaxy, it has become a customary to consider a hidden pair of capacitor and inductor inside. In the 1990s, the quantum versions of these pairs arrived as a quantum capacitor and quantum inductor, now we wire them classically to find the quantum resonance. It is astonishing, since the violation of Kirchhoff's law was proposed in the 1960s, that the current-times-resistance of all the elements in a closed loop must equal zero, if not, for example, emission by any element, the time-varying magnetic field generating additional input, then the law violates. Most importantly, if there is a device architecture in which there is a device inside a device, or the escape time fractal-like hardware—the central hallmark of this book, again the Kirchhoff law would be violated.

How to emulate coherent emission It is shown now that if we wire the quantum elements in series or parallel, the conductances do not add up (Gabelli et al., 2006). The culture of obtaining the resonance frequencies by a linearly wired resistor, capacitor, and inductor still continue. Since in a quantum inductor, a magnetic flux generates by reflection and not by current flow, and in a quantum capacitor forms without storing a real charge, both the magnetic flux and the charge were neither quantified nor detected. These quantum elements originate in the quantum well embedded inside a classical capacitor, not alone, as an original device. In the quantum well, a wave function not only interacts with the input electromagnetic wave (Aharonov and Bohm, 1959), but also emits entangled photons at room temperature (Michler et al., 2000), the effect of magnetic and electric dipoles are explicitly distinguished in the interference pattern (Freed and Weissman, 1941). In a quantum well, even the physical oscillation of a trapped charge could repeatedly emit coherent quantum bursts of infra-red surviving longer than picoseconds (Roskos et al., 1992). Remarkably, a superlattice of quantum wells is more stable in the coherent emission for both electromagnetic (Waschke et al., 1993) and magnetic spin wave (Oh et al., 2017). It promises designing an array of quantum antenna that could shape how the emitted ripple would look like. Until now, enhancing magnetic emission by suppressing the electrical emission was achieved by introducing a pseudo level (Karaveli and Zia, 2010). Advancing further, if the oscillating charge of a quantum well could reshape the electromagnetic wave into a packet of coherent magnetic flux, then a wireless burst of magnetic ripple could flow like a photon through the medium or even vacuum. An extreme environment would not be required to run the quantum coherent circuits. One would not require to build a parallel, or series wiring of quantum device. The quantum elements could float at proper orientation at the coordinates so that all the participating circuit

elements build a combined phase space. An integrated chip would look like a 3D geometric shape where no current flows. The route is unique among all existing proposals to survive quantum effects in an ambient condition since it suggests rearranging the classical environment as a unique topology of quantum's infinite choices requires.

An electrical charge cannot flow since we want the magnetic vortex atom to flow as pure evidence, a solution to such critical demand were made in the 1990s. Increasing the dwell time of an electromagnetic wave in a well could mean the storage of charge like a capacitor C_q and if the wave repeatedly reflects between the walls of a potential well could generate a circular current flow like an inductor L_q . These are not normal capacitor and inductor, and the origin is not geometry but discrete energy levels of a material. In order to satisfy Dirac's criterion, the unique potential well acting as L_q and C_q should act as an antenna that would radiate a magnetic ring or torus outside the potential well. For that to happen, the height of the potential wells should vary, not directly with the real charge but a parameter that controls the dwell time of an electromagnetic wave trapped in a potential well, obviously, it is frequency. Unfortunately, the wall parameters of quantum wells are fixed as soon as it is fabricated, so we need to design a virtual quantum well just like the concept of an artificial molecule was engineered.

The height and width of the walls of the virtual well made of charge varies alone to regulate the emission of classical or quantum rings of magnetic flux. That is why single microtubule's capacitance oscillates as a function of length, pitch and diameter (Figure 8.9a–c). Does the storage of charges change the spiral? In order to find an answer, we calculated quantum capacitance, $C_q = \partial Q / \partial V = \partial Q / \partial \psi$. We solve equation (8.15) to find the expression of quantum capacitance of the system,

$$C_q = \frac{vm^*q^2}{2\pi\hbar^2} \left[2 - \frac{\sinh(E_g/2kT)}{\cosh\left(\left(\frac{E_g}{2}-q\psi\right)/2kT\right)\cosh\left(\left(\frac{E_g}{2}+q\psi\right)/2kT\right)} \right].$$

When C_q is measured using a differential bridge circuit; the theory is found consistent with the experimental result. The actual charge stored in the wall could be measured using C_q directly. Using a semiconductor electron emitter we injection charge to the protein and applied nT range magnetic flux, we could not change the flux density image. The ring and spirals are not made of charge or spin, as conventional magnetic fields are defined. The effective mass of the massive carriers trapped in the lattice cells was measured experimentally on the single microtubule and experimental data provides clear evidence that the effective mass increases as we trap more (Figure 8.9d).

In order to confirm that the emitted magnetic flux is truly ring-shaped, first we consider that there is truly a ring, on its perimeter at any point, $\psi(t) = \psi \sin \phi$; then due to the quantization of a circular path $\phi = \frac{2\pi}{\Phi_0} Q$, where Φ_0 is the magnetic

flux quantum in the ring, we get the quantum inductance $L_q = \frac{\Phi_0}{2\pi Q} \frac{1}{\cos \phi}$. Then, from the density of states, we recalculate quantum inductance $L_q = \frac{\hbar^2}{12\pi q^2 \Gamma_L}$. Both the expressions of quantum inductance calculated from the density of states and ring topology give the same value which suggests that there is truly a ring and it originates in the virtual quantum well. Also, since in a generic quantum well $L_q = \hbar / 2\Gamma G$, earlier, conductance G was related to current flow, here a comparison shows $G = \partial Q / \partial \psi$. The finding suggests a new paradigm of transmitting energy as rings of magnetic flux, which experiences a new kind of resistance, primarily topological. By arranging seeded quantum wells in a particular geometry in the 3D space filled with extremely insulating matrix ($R = \infty$) one could build artificially integrated chips of non-electronics, where another resistance is $H = 0.001$. Quantum conductance and quantum inductance were measured on a single microtubule (Figure 8.9e, f), which showed that not just one, single microtubule exhibits multiple such values, and one could regulate or tune those values using simple control parameters. The measuring device is shown in Figure 8.9g. It seems beyond electronics we may have an era of super non-conductivity (Figure 8.9h).

8.5.1 THE CONCEPT OF PHASE SPACE WITH 12 HOLES THAT BLINK

Twelve singularities of combined phase space: Opening and closing the undefined holes on the phase sphere: The wave $\vec{\psi}_{mag}$ from Ω number of cells interfere, the boundaries set by D, P, L, and ab adds wave functions from three directions (${}^3\Sigma_i \cos x_i$) and takes a product from two directions (D, L) with a feedback effect (${}^4\Pi_i \cos x_i$). So, we get the number of reflections $\Psi \sim \tau e^{\Omega {}^3\Gamma_i(r,t)} / c_m$. That equates a delay τ ($\sim \Delta Q$, delay=charge, no real electron storage) with the magnetic flux produced, hence $H = \frac{\Delta \Psi}{\Delta Q} = e^{\Omega {}^3\Gamma_i(r,t)} / c_m$. Oscillating L, P, D, and ab delivers the phase factor $\Gamma_i(r,t) = 3 \sum_i \cos(x_i \cos t_i) + 4 \prod_i \cos(x_i \cos t_i)$; x_i is replaced by the geometric parameters. In a Hinductor device or H, the phase sphere an equivalent to the Hilbert space of a qubit has 12 singularities. It means it has 12 holes on the sphere (Figure 8.9i, j). There are a pair of singularities for all six x, y, z, xy, yz, zx directions, so we get 12 holes. The generic function that regulates the solutions is given by $3 \sum_i \cos \theta_i + 4 \prod_i \cos \theta_i$. However, there is a temporal function added to the angular values in this function $\cos \rho_1 \cos \rho_2 \cos(\rho_3 \sin t)$, or $\cos(\rho_i \sin t)$. When discrete magnetic rings $\Psi_1, \Psi_2, \Psi_3 \dots$ holding a geometric shape change the diameter, actually on the phase space the holes of singularity change their diameter. It is a beautiful life-like event. As electric field clocks the magnetic ring, the solid angle ρ_i created by phase singularity oscillates as a function of time $\rho_i \sin t$, but we can add 1–12 temporal functions in $(2^n - 1) \sim 4 \times 10^3$ ways. Thus, a fundamental Hinductor device carries out 4047 distinct temporal dynamics. A maximum of 12 vertices solid 3D topology it can represent, e.g., hexagonal prism, icosahedron, triangular bifrustum, truncated tetrahedron, etc. If Ψ_1, Ψ_2, Ψ_3 triangle's all three rings oscillate due to electric

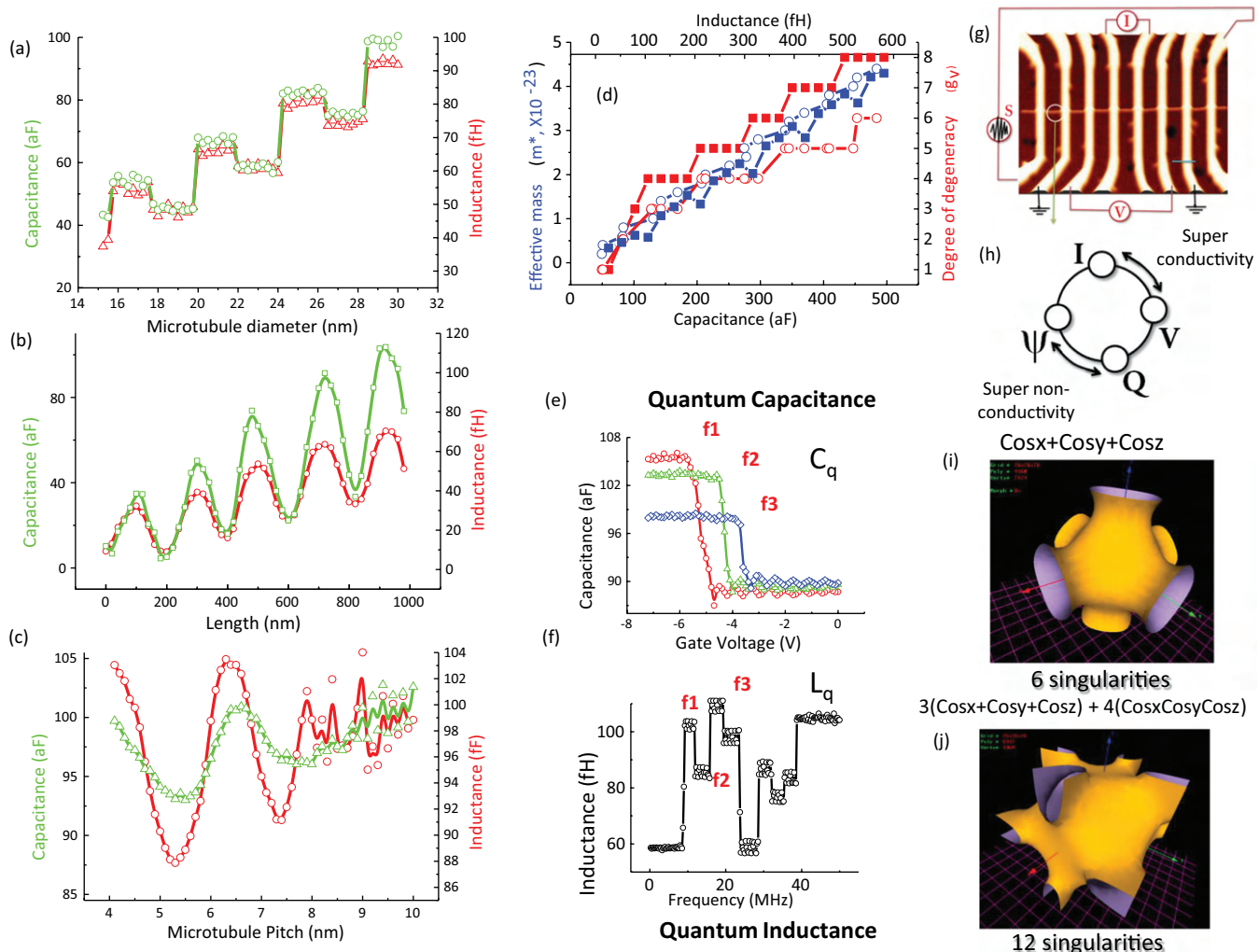


FIGURE 8.9 Three panels (a), (b) and (c) show that the variation of capacitance of a microtubule as a function of its diameter, length and pitch. Capacitance was measured at 1 kHz. (d) Effective mass and degree of degeneracy of the magnetic particle-like vortex produced in the junction of two cylindrical layers of microtubule. Both inductance and capacitance were measured plots at 8, 16, and 22 MHz capacitance variation as a function of gate bias. Quantum measurements were carried out using a bridge circuit. (e) Quantum capacitance or capacitance inside a classical capacitor was measured for microtubule for three different frequencies. (f) Quantum inductance is plotted for three different frequencies. (g) E1-E8 Au electrodes on SiO_2/Si substrate is grown, microtubule is spray injected perpendicular to the E1-E8 electrodes. Electrode noise is applied from source S, via E1-E8 pair of electrodes. E2, E7 are ground to restrict leak current flow further. E3, E6 measures voltage, E4, E5 measures current integral or charge. E3-E6 is used as capacitance bridge, and inductance bridge for all measurements. Scale bar 300 nm. (h) Just like superconductors are diamagnetic, all H devices tend to become super-non-conducting. (i) The 3D plot of the function $\text{Cos}x + \text{Cos}y + \text{Cos}z$. (j) The 3D plot of the function $3(\text{Cos}x + \text{Cos}y + \text{Cos}z) + 4(\text{Cos}x\text{Cos}y\text{Cos}z)$.

field fluctuation ($\partial E / \partial t = \partial \phi / \partial x$), since an angle between Ψ_1, Ψ_2 as $2\pi\phi_{12} / \phi_0$, then three angles of the triangle clocks as a single entity. Thus, clocks bind.

We get a plug-n-play expression for $H = \frac{1}{C_m} e^{\Omega^3 \{ \Gamma_i(r,t) \}}$ equation (8.10), input device geometry and stored charge or frequency, get magnetic flux as output. $\Gamma_i(r,t)$ has 12 singularity domains, i.e., holes in the phase space. It means for certain L, P, D, ab values, undefined or no amount of magnetic flux is generated by the device. Here cost_i estimates a periodically oscillating geometry say L, P or D, then the associated hole is bridged. Moreover, N frequencies of G-mode, each defines a combination of $\cos t_i$, which sets the boundary

of a hole, that edge shapes the geometry of the magnetic vortex produced. We find below how to read information content (G-mode) written by a user ($\hbar\omega$) using the blinking of holes as a vortex synthesis mechanism.

8.5.2 PERIODIC OSCILLATIONS WITH LENGTH, PITCH, LATTICE AREA/DIAMETER—THEORY AND EXPERIMENT

In Figure 8.9a–c, we present a simple study that the capacitance of microtubule changes as a function of its length, pitch and diameter. Now, since, we saw above that one could open or close 12 holes in the phase space, varying only geometric

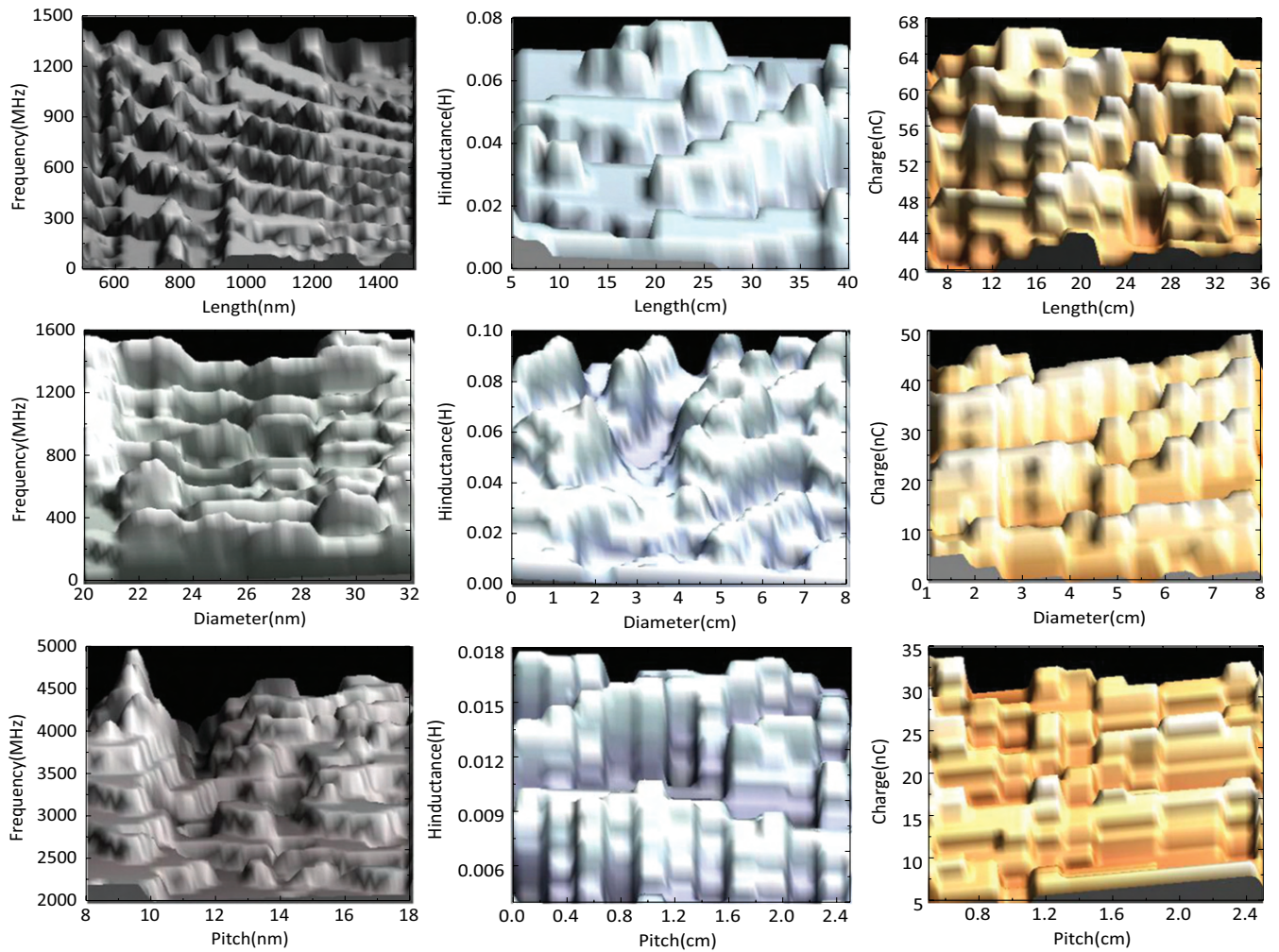


FIGURE 8.10 There are three columns. The first column is the theoretical length pitch and the ratio of lattice area/diameter variation for the microtubule. The second column is the H variation as a function of length pitch and the ratio of lattice area/diameter experimental data. The third column is the theoretical prediction for the artificially synthesized H device charge storage calculation as a function of length, pitch and the ratio of lattice area/diameter.

parameters, length, pitch, diameter, it is time to dig deeper. Figure 8.10 shows three plots, microtubule's, resonance frequencies, H and stored charge variation as a function of geometric parameters. The plots show that Tomasch oscillation like periodic changes is a universal feature of charge-magnetic flux response of a device. The periodic oscillation means for charge-flux operating particles, or magnetic rings or magnetic vortices, the extreme insulated cylinder acts as an H -less device. Thus, we could now sum-up basic arguments why H might claim to be a fourth-circuit element (Figure 8.11a).

In the quantum model of the fourth-circuit element device, namely microtubule, a pair of α -helices of a tubulin protein molecule forms a quantum well, a different number of coils of an α -helix act as asymmetric barriers ($n = 4, 7.8 \text{ cm}^{-1}, 12.4 \text{ cm}^{-1}$). The water molecules between a pair of helices generate a pair of shallow, deep quantum well. Water's quantum well is the guest in the host α -helix quantum well. Vibrational frequencies of water and helices are calculated by DFT for $n = 4$ and

$n = 2$ loops and 12 water molecules in between. Depending on the type of protein and its concerned group of α -helices, the values of squeezed states change. The Schrödinger's equation for an arbitrary non-stationary state of the wave function in this virtual well is $\Psi(q,t) = \sum a_n e^{-\frac{i}{\hbar} E_n t} \Psi_n(q)$, the coefficients satisfying the normalization condition $\sum |a_n|^2 = 1$; coefficients are determined if $\Psi(q,0)$ is known and $\Psi_n(q)$ are orthonormal. For time-dependent Schrödinger equation $i\hbar \frac{\partial \Psi}{\partial t} = -\frac{\hbar^2}{2m} \frac{\delta^2 \Psi}{\delta q^2} + \frac{1}{2} kx^2 \Psi$. The ground state solution is the wave function is $\Psi(q,0) = (\alpha^2/\pi)^{\frac{1}{4}} e^{-(\alpha(x-a))^2/2}$. At high temperature, we replace α with a new arbitrary constant β , so that the wave function becomes $\Psi(q,0) = (\beta^2/\pi)^{\frac{1}{4}} e^{-(\beta x)^2/2}$. Ground and noise-driven higher states only differ by its height and width. If we calculate a_n and sum up the series, we get Schrödinger's equation for a non-stationary state $\Psi(q,t) = \frac{\alpha}{\pi^{1/4}} \sqrt{\frac{2\beta}{A+B\zeta}} \exp\left(-\frac{i\omega_c t}{2} - (\alpha x)^2/2 \frac{A-B\zeta}{A+B\zeta}\right)$, where $A = \alpha^2 + \beta^2$, $B = \alpha^2 - \beta^2$, $\zeta = e^{-2i\omega_c t}$. The coordinate probability density $\Psi\Psi^*$ is now

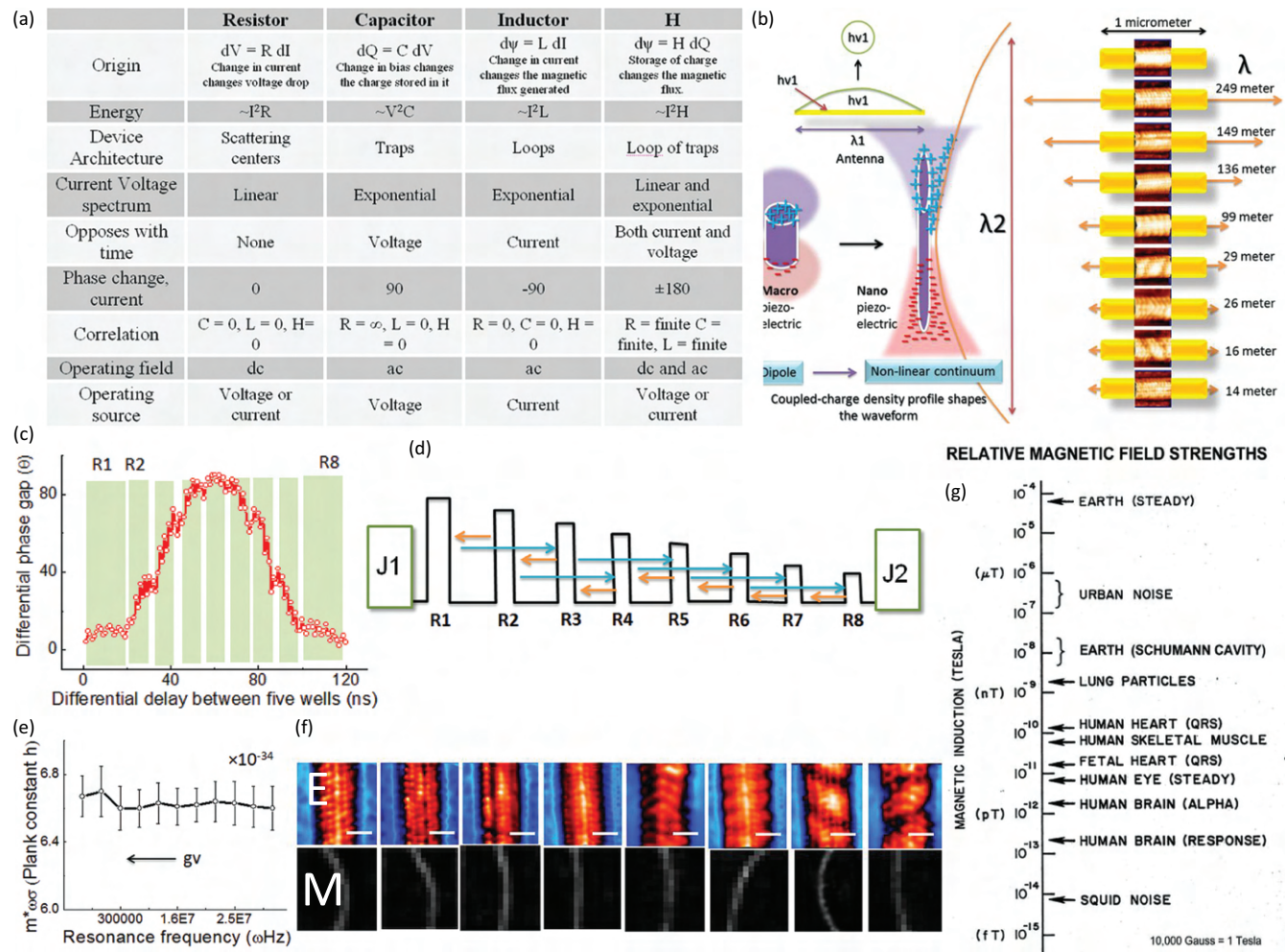


FIGURE 8.11 (a) Comparison between different fourth-circuit elements. (b) Eight different long-wavelength magnetic waves created on the microtubule surface are estimated when wirelessly electromagnetic signals were pumped on the microtubule. (c) Using probe of Figure 8.9 (g), in its measuring circuit, phase gap between phase ahead and phase lag wave is plotted as a function of time, simultaneously the magnetic flux is recorded, which shows quantized jumps. The wavelike variation (MHz) is theoretically fit. Five electrodes (C1–C5) are wired as phase array connected to magnetic wave on the microtubule surface shown in panel f. InP connected Pt electrode is used to sync clocking, ensuring phase array response. The Del1-Del2 goes to phase-locked loop differential amplifier, which measures differential phase gap plotted below as a function of time. (d) Schematic of octave of octave ripples integrated into one is shown as resonant tunneling diode. (e) Effective mass, resonance frequency, and cross-sectional area of microtubule for different degree of degeneracy generate the Planck constant. This is fractal quantization process. (f) Comparative electronic density of states (edos) and magnetic flux measurement (27 pixels as rectangles) using coaxial atom probe, for tubulin monomer (scale bar 0.2 nm); tubulin dimer (scale bar 1.8 nm); microtubule (scale bar 6 nm). (g) A chart showing naturally found material's magnetic field.

$$\rho(q,t) = \frac{\alpha^2 \beta}{\sqrt{\pi}} \sqrt{\frac{2}{\alpha^4 + \beta^4 + (\alpha^4 - \beta^4) \cos 2\omega_c t}} \exp\left(-\frac{2\alpha^4 \beta^4 q^2}{\alpha^4 + \beta^4 + (\alpha^4 - \beta^4) \cos 2\omega_c t}\right)$$

through the virtual well ($k_0 = E$), absorb ($k_{+1} = E + \hbar\omega$), or emit ($k_{-1} = E - \hbar\omega$) a wave packet from the wells of helix or water. The transmitted wave function from the virtual quantum well

$$\vec{\Psi}_{trans} = \left(t_0 e^{ik_0 z} + t_{+1} e^{ik_{+1}(z+\omega t)} + t_{-1} e^{ik_{-1}(z-\omega t)} \right) e^{-\frac{iEt}{\hbar}} = \vec{\psi}_{Osci} + \delta \quad (8.13)$$

The center of the wave packet remains confined, but the wave packet oscillates periodically with its width and height, similar to a classical dipolar antenna $\rho(q,t) \sim \sin^2 \omega_c t$. The periodic quantum oscillation takes a torus or ring shape, it can tunnel

The transmitted wave through the virtual well $\vec{\psi}_{Osci}$ and a part of it emitted as infra-red δ are in the same phase ($\phi_{\pm 1}$); it is calculated adopting Breit-Wigner form of transmission at around resonance (E_R)

$$\phi_{\pm 1} = \phi_{\pm 1,0} + \tan^{-1} \frac{E - E_R}{\Gamma} - \tan^{-1} \frac{E - E_R \pm \hbar\omega / 2}{\Gamma} \\ + \tan^{-1} \frac{E - E_R \pm \hbar\omega}{\Gamma},$$

where Γ is the width of the resonance peak for both, $\vec{\psi}_{Osci}$ and δ .

An infra-red sensing nanowire and a magnetic flux sensing nanowire located at the tip of an atomic resolution probe is brought to the atomic scale vicinity of the protein, simultaneously detects this phase in two independent signals, one electromagnetic and another, magnetic. Instead of interferometric detection of coherent infrared emission, or electro-optic gating, Ghosh et al.'s dual-mode nano-sensor remains a ~4 nm apart from the emission center, by reducing detection energy to 10 μ V from 10 meV, fit to sense coherent burst 1–2 ps (10^{-12} seconds); and magnetic flux sensitivity (nT to 0.1 pT). Measuring the magnetic flux of an electromagnetic burst is critical since M-field is 10^4 times less than E-field at the sensor (Burresi et al., 2009). They detect M-field because it is a magnetic ring that resonates with the magnetic nanowire. Often the microtubule boundary is such that the waveforms do not end at boundary, the vibration around boundary is such that effective waveform is much longer (Figure 8.11d).

The oscillatory part of the magnetic flux is calculated by considering a geometric series of amplitude t , which changes due to a repeated reflection of $\vec{\psi}_{Osci}$ between the two walls of a virtual well. In the geometric series of t the number of higher-order terms we consider is proportional to the height of the virtual well, i.e., a function of stored charge (Karaveli and Zia, 2010).

$$\vec{\psi}_{Osci} = \frac{\partial \vec{\psi}_{static}}{\partial Q} \left[1 + \left(\frac{\hbar\omega}{2\Gamma} \right)^2 \right]^{-\frac{1}{2}} Q_{osci} \cos(\omega t - \alpha) \Theta(E_R) \Theta(E_F - E_{\pm 1,0}) \quad (8.14)$$

The above expression is calculated for three reflections, links charge, and magnetic flux directly. Using the coaxial nanosensor, we apply 0.2 THz sinusoidal pulse to the THz nanowire sensor. The pulse stream traps the oscillating charge, we get Q_{osci} , that creates a ripple in the magnetic flux measured by the nanowire sensor, thus, we get $\frac{\partial \vec{\psi}_{static}}{\partial Q}$, experimentally. The differential phase gap, measured by sending picosecond pulse streams is plotted in Figure 8.11c, which shows eight ripples possibly from eight local density of states observed in the tubulin protein. Eight wells are shown schematically in Figure 8.11d. When the externally applied resonance frequency was varied to selectively activate a particular well, the effective mass was found to be constant (Figure 8.11e). It suggests that the magnetic vortex-like structure is a fundamental unit of signal and we could use a quantum wave function to operate or manipulate it. From the wave function ψ reflecting

between the virtual walls of alfa-helices and the water well, we calculate the amount of charge contained in the virtual walls of the virtual well.

$$Q = \int_0^\infty g(E) \left[f\left(E + \frac{E_g}{2} + q\dot{\psi}\right) - f\left(E + \frac{E_g}{2} - q\dot{\psi}\right) \right] dE \quad (8.15)$$

Considering a parabolic band, $g(E) = \frac{m^*}{\pi\hbar^2} v(E)$, where $v(E)$ is the number of energy levels of the virtual quantum well's wall, which are occupied.

Charge Q (equation 8.15) is used to calculate the emitted or radiated part $\vec{\psi}_{Osci}$ (2), hence we get $\vec{\psi}_{Osci} \propto \cos(\omega t - \alpha)$ experimentally. The comprehensive match between (2) with the experiment suggests that Sahu et al.'s quantum well model works in coupled α -helices of a protein. The magnetic flux is emitted all around the 3D structure as $\vec{\psi}_{Osci} \vec{\psi}_{Osci}^* = \rho(q, t)$, there are four primary and four minor quantum wells in a monomer as estimated by quantum tunneling measurement of the local charge density of states.

An extreme insulator, microtubule's resonant oscillations are topologically similar to its constituent protein tubulin's resonance band, which are also extreme insulators. They all could be switched to a super non-conducting state simply by applying noise. By constructing a special coaxial atom probe, one could detect thermal and magnetic flux signals simultaneously. It has been observed that the pairs of quantum capacitance and quantum inductance generate geometric resonances in a single brain extracted microtubule. Microtubules magnetic phase nests its dimers phase that nests its monomer's phase, a grouping of atomic-scale waves continues to form larger waves is neither seen in classical nor in quantum (Figure 8.11c). So, we can neither take a product of monomers wave functions to generate the wave function of a microtubule nor can we use existing quantum formulations as is. The super non-conductor generates a giant quantum magnetic flux like a superconductor (Figure 8.11f).

8.5.3 KNOTS OF DARKNESS ON THE H INTERFACE

In order to confirm the formation of knots of darkness on an H surface, the protein surface was scanned using the magnetic nanowire, and the formation of magnetic spiral in the monomer was confirmed (Vignolini et al., 2010; Figure 8.11f). The confirmation continued when the monomer forms a dimer and even when it makes a giant protein complex. The measurement was repeated for tubulin protein, actin, and clathrin and checked for the non-existence of such behavior in a single-walled carbon nanotube, but present in a helical multiwalled carbon nanotube. Magnetic fields are reported in many biomaterials, often this is due to magnetic materials. What magnetic features we observe in fourth-circuit element or by synthesis of light do not require any magnetic material (Figure 8.11g).

The cell traps $\vec{\psi}_{trap}$ emits, $\vec{\psi}_{osci} = \frac{1}{4\pi^2} \int_0^{k\omega_c} \vec{\psi}_{trap} dk (\frac{k+1}{k+1}^2 - \frac{k-1}{k-1}^2) \times \vec{j}$, is integrated over 360° solid angle around a cell (ϕ = precision, θ = deviation due to paraxiality on an anisotropic path, α = relative perturbation angle). Since at singularity ($E = E_R(r, \theta, \phi)$), $\phi_{\pm 1} = \phi_{\pm 1,0} + \tan^{-1} \frac{E - E_R}{\Gamma}$, (Γ is resonance peak width, E_R energy of a resonating cell made of (na, nb), n is an integer, a, b are lattice parameters, +1 means higher energy state, -1 means lower) contributes in the vertical z -axis primarily, we get $\vec{\psi}_i = \vec{\psi}_{osci} \cos \alpha \cos(\tan^{-1} \frac{E - E_R}{\Gamma})$; $\vec{\psi}_j = \vec{\psi}_{osci} \sin \alpha \cos(\tan^{-1} \frac{E - E_R}{\Gamma})$; $\vec{\psi}_k = \vec{\psi}_{osci} \sin(\tan^{-1} \frac{E - E_R}{\Gamma})$. The plot of

$$\vec{\psi}_{mag} = \hat{i}\vec{\psi}_i + \hat{j}\vec{\psi}_j + \hat{k}\vec{\psi}_k \quad (8.16)$$

is a 3D spiral connecting the localized phase singularities on an oscillating sphere. This spatial structure is carried by a light like signal ($E \ll B$). The plot of these distributions is a spiral connecting the localized phase singularities, if other quantum elements are placed on the stationary state solutions locate on this path, it will contribute to the Hilbert space as a singular solution.

From the above expression of $\vec{\psi}_{osci}(i, j, k)$, we get the equation of a circle when $E = E_R$, thus, we derive the formation of a ring of magnetic flux, by two independent theoretical formulations. First formulation deals, when a shot noise $\langle \omega_c \rangle$ is absorbed into quantum oscillations ($\rho(q, t)$). Second formulation deals, when the virtual well is pumped with its resonance frequency. All along the spiral path of the magnetic flux, the measuring nanowire senses a quantized increment of flux, as the system is charged with a photo-induced electron emitter; thus, $\Psi = HQ$ has both, a classical and a quantum version. To underpin the lensing effect, Sahu et al. measured the density of states for alpha-helix well and water well; one has to read d^2I/dV^2 and $d^2Q/d\Psi^2$, which shows that the magnetic density of states is at the boundary of the electromagnetic density of states. By de-phasing during a scan using noise, we track the diffusion σ of magnetic flux. Thus, the ring is made of electromagnetic wave wherein $|\vec{E}| \ll |\vec{B}|$, it is classical if $\frac{\hbar\omega}{\Gamma} \ll 1$. Proteins do exhibit quantum effects at room temperature, under massive noise. However, here, the concerns of de-phasing by scattering do not exist. It is all about the topological 3D orientation of quantum wells on the surface of a 3D phase sphere, as $\cos \alpha$ regulates not just the basic ring formation, but, stabilization by assembling the rings in a spiral form. Not just tubulin, actin, all the proteins whose beta-sheet forms a spiral at the backbone, may exhibit flux-ring condensed wave.

8.6 THREE INTERACTIVE CYLINDERS PERTURBING THE KNOTS

At least three concentric cylinders is a unique engineering feature of Hinductor. Multilayer coils enhance wireless transmission (Nair and Choi, 2016). Each layer generates distinct waves, the inner coil k_i^* , and outer coil k_o^* , both 180° out of phase sources perturb the central coil's straight stationary dark line, D_c , with wave vector k_c^* at an angle α and build singularity structures D_i and D_o respectively. D_c , D_i , and D_o are identical dark lines, differ by diameter alone, and hence trigger beating. We plot beat pattern. The dark lines interact depending

on the polarization. The dark lines ($E_t = (E_x, E_y) = 0$) form when the real parts of propagating signal $kr'e^{i(\theta'+\zeta)}$ and the two perturbation signals from $e_1(e_1 e^{i(k^* \cdot r - \omega t)})$ and $e_2(e_2 e^{i(k^* \cdot r - \omega t + \Delta)})$ generated by the central coil's screw and edge dislocations cancel each other. Different zig-zag paths generate distinct pairs of e_1 and e_2 . We express e_1 and e_2 as $\bar{e} = (e_1 + e_2)/2$ that represents total strength of perturbation and $\Delta e = (e_2 - e_1)/2$ that represents polarization ($E_x \neq E_y$). Interactions of dark lines could change e_1 and e_2 , they could make a circle, or ellipse or even magnetic rings or vortices (Figure 8.12a, b).

Under noise, $\hbar\omega$ activates all three layers (Figure 8.12c), we scanned the knots on the surface using a magnetic flux microscope and theoretically fit the common bright region between two modes to find the covariance matrix of $\vec{B}(x, y)$ and $D(s, \theta')$, namely φ , and the coupled wave function Ψ_l using $\mathbf{H}\vec{\psi}_{mag} = \Psi_l(l_i, t)\Psi_l(l_i, t)H$, where \mathbf{H} is Hamiltonian, equation (8.8) gives H , $\vec{\psi}_{mag}$ is calculated from equation (8.16), and $\Psi_l(l_i, t) = B_i \exp(i\omega t)$, where $B_i = I \langle \vec{B}(x, y) \rangle A$, A is the area on the surface where G-mode i is active, I is the periodicity index. To explain how magnetic vortex-like particles could cover the surface area, we start with three concentric layer cylinders, S1 falls on the top spiral, creates two coherent sources (Figure 8.12c). One part S2 again creates a pair of coherent sources at the junction of second and third spiral (Figure 8.12c). The critical condition that creates magnetic particles is squeezing the first knot of darkness, if we squeeze more by changing Δe . These free magnetic particles could rotate clockwise or anticlockwise (Figure 8.12c). The coherent sources created by S1, S2, and S3 interfere and generate composition of patterns of magnetic vortex on the cylindrical surface (Figure 8.12d). When wave functions of two simultaneous situations created by S1-S2 and S2-S3 are superposed and that builds the unit time crystal (Figure 8.12e).

Generalized orbital angular momentum generation and Holographic projection of time crystal as a set of orbital angular momentum set: Spiral dark lines, randomly arranged in the 3D space, were theoretically predicted by $D(s, \theta')$ and routinely observed for four decades. Now the same spirals with modified OAM contain the coupling coefficients CC_i and the wave vectors of distinct G-mode frequencies. Here at $\hbar\omega$ triggered G-mode resonance, the induced Δe varies periodically $\Delta e = \sin \delta$, then angle α switches sign periodically, the dark knots assemble in a singular pattern of topological charge $l = il_1 + jl_2$, $\Psi_i(l, t) = D_i(s, \theta') \times \exp[2\pi i \frac{\varphi_{l_1+1}}{\varphi_{l_1}}] \times \Psi_{l_1}(l_i, t) = C_i(r, t)$; i.e the collective oscillation of three cylinders integrate the knots. To predict the experimental output, we derive a projection function

$$P(r, t) = \sum_{i=1}^N \Gamma_i(r, t) \times \Psi_i(l, t) = \sum_{i=1}^N C_i(r, t) \dots \quad (8.17)$$

as a product of the phase space $\Gamma_i(r, t)$ and 3D coordinates of dark lines containing N number of G modes. $P(r, t)$ binds N number of magnetic dark knots which are allowed by a phase space $\Gamma_i(r, t)$; it creates a nest of N number of 3D assembly of

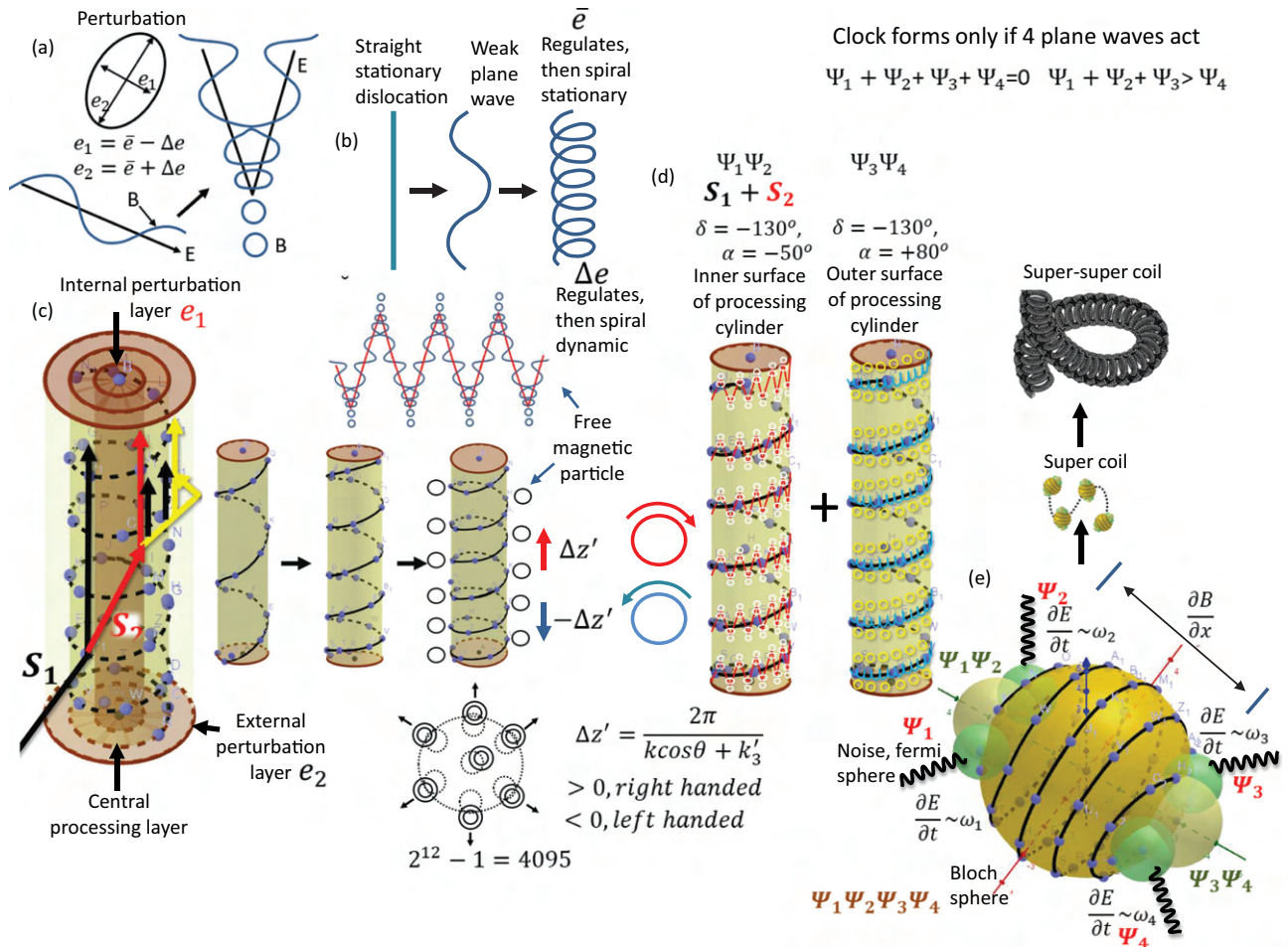


FIGURE 8.12 (a) Defining polarization of perturbation. $\Delta e = 0$, means no polarization. $\delta = \pi/2$, edge dislocation, $\delta = 0, \pi$ left- and right-handed screw dislocation. When two E lines interfere with disappearing, we find magnetic rings. (b) If the H device surface changes lattice profile due to external resonance, then the dislocation also oscillates, polarization also oscillates and a spiral dynamics of dislocation forms. (c) Three sources S_1 , S_2 , and S_3 from three layers form, S_2 and S_3 from inner and external layers, which perturbs the central layer S_1 . The dark lines formed on the 2D surface of H device deform and generates rings. The rings formed on the surface of H device is projected to the screen 4095 ways. On the H device surface dynamic spiral knots rotate clockwise or anticlockwise. (d) The loops and knots formed between S_1-S_2 interface and S_1-S_3 interface are shown, which eventually emits particle-like magnetic structure in the panel (e). Four periodically oscillating magnetic loops bind into the 3D particle-like magnetic flux distribution as shown in the panel (e).

2D rings. Each vortex crystal has N number of OAMs or vortex atoms, each with a topological charge $l_i = I_i m \exp[2\pi i \frac{\varphi_{l+1}}{\varphi_l}]$. The 2D projection of magnetic vortices is $P(r, t)$ or $\sum_{i=1}^N C_i(r, t)$ created by multiple materials on magnetic films. Magnetic 3D vortices pass through even if the optical vortex is blocked using a black carbon sheet. A magnetic vortex reflects in the mirror, moves through the water or a non-magnetic plastic, bends by a magnet etc.

8.6.1 KNOTS OF DARK LINES ACT LIKE A SPIN OF A PARTICLE

Phase singularity or phase discontinuity has become a major point of discussion in the recent times due to the manipulation of angular momentum of light and other properties using light-matter interaction (Genevet et al., 2012). The basic laws of reflection and refraction are modified (Yu et al., 2011). Geometric

parameters of a helix are responsible for the phase singularity or phase discontinuity (Huang et al., 2013a, 2013b). In case the surface has a metamaterial property, anisotropic transmission of electromagnetic signals along the surface enables out of plane reflection and refraction of light (Aieta et al., 2012). One of the most exciting parts about this phase singularity or phase discontinuity is that it is dispersion-less, which means, one the propagating light build up a singularity, that angle would not change while passing through the material (Huang et al., 2012).

Out of three concentric coils, central one processes, the inner and outer coils perturb (Figure 8.12c). Since coils are twisted, mixed screw and edge dislocations on the YZ plane of coil surface is realized by rotating x-axis by angle δ , so that YZ plane rotates by δ , $(x, y, z \rightarrow x, y', z'; k \rightarrow k^*, i.e. k_1, k_2, k_3 \rightarrow k_1, k'_2, k'_3)$. Each layer generates distinct waves, the inner coil k_i , and outer coil k_o^* ,

perturbs the central coil's straight stationary dark line k_c^* at an angle α and build singularity structures D_i and D_o , respectively. Inner and outer coils are internal and external mirrors, act as a pair of 180° out of phase sources, thus, fit to edit perturbation phase 0° – 180° and 180° to 360° . Splitting of light into the isolated optical and magnetic vortex is achieved by tuning α , to do that the relative position of inner and outer coil shifts with respect to the central one. Three concentric spiral cylinders are in contact via yz plane, hence, k lies in the yz plane making an angle α with Oz , sign positive toward Oy , we can simplify above equations $k_1 = 0$, $k'_2 = k \sin(\delta + \alpha)$, $k'_3 = k \cos(\alpha + \delta)$ and from this identity we get $(kr')^2 = (e_1 \cos(s))^2 + (e_2 \sin(s + \Delta))^2$, which gives r' , average radius of loops like circles and ellipses. To find knots or zero level contour, or spiral dark knots with radius $\Delta e/k$ we find s, θ' , here, $D(s, \theta') = kr' \cos(\theta' + \zeta) + e_1 \cos(s) = 0$; wherefrom we find s, θ' convert $D(s, \theta') \rightarrow D(y', z')$, it contains wavefunction $\Psi_i(r, t)$ of OAM set.

Equation (8.17) links a shape-changing vortex or a helical nanostructure with the geometry of its 3D magnetic vortex output. To experimentally verify this, we shine a polarized 633 nm laser light on the solution of a helical nanowire, dendrimer, helical gel, etc. kept in a quartz cell, the light is passed through

a $\lambda/4$ plate vortex lens for 400 nm, not 633 nm (Figure 8.13a, b). If we use 400 or 800 nm laser, the optical vortex is strong, but at 633 nm a mismatch makes the system unstable and subtle changes in the magnetic vortices are distinctly reflected. Output magnetic vortex is projected on two types of films, Ni or Fe microwires dipped in oil microsphere, long exposure (>2 hours) changes the film color, bright rings map a 2D slice of the 3D magnetic vortex. The separation between the magnetic and optical vortex 5 m away from the sample is around 15 cm, it depends on the angular relation between reflector, sample and vortex lens. On the sample we shone $\hbar\omega$ using a Yagi antenna and estimated the stored charge Q on the surface and magnetic flux on the film as a function of L , D , P , and ab by two separate experiments. The change in capacitance with the voltage at different ac frequencies gives Q .

8.6.2 SYNTHESIS OF SUPER-SUPER COIL MADE OF DARK LINES

When both \bar{e} and Δe are present, \bar{e} tries to form a static helix and Δe tries to form a dynamic helix. If $\Delta e < \bar{e}$, i.e., ($e_2 < 3e_1$) the static helix acts like a guideline on which another dynamic helix forms, we get a supercoil. If additional perturbation

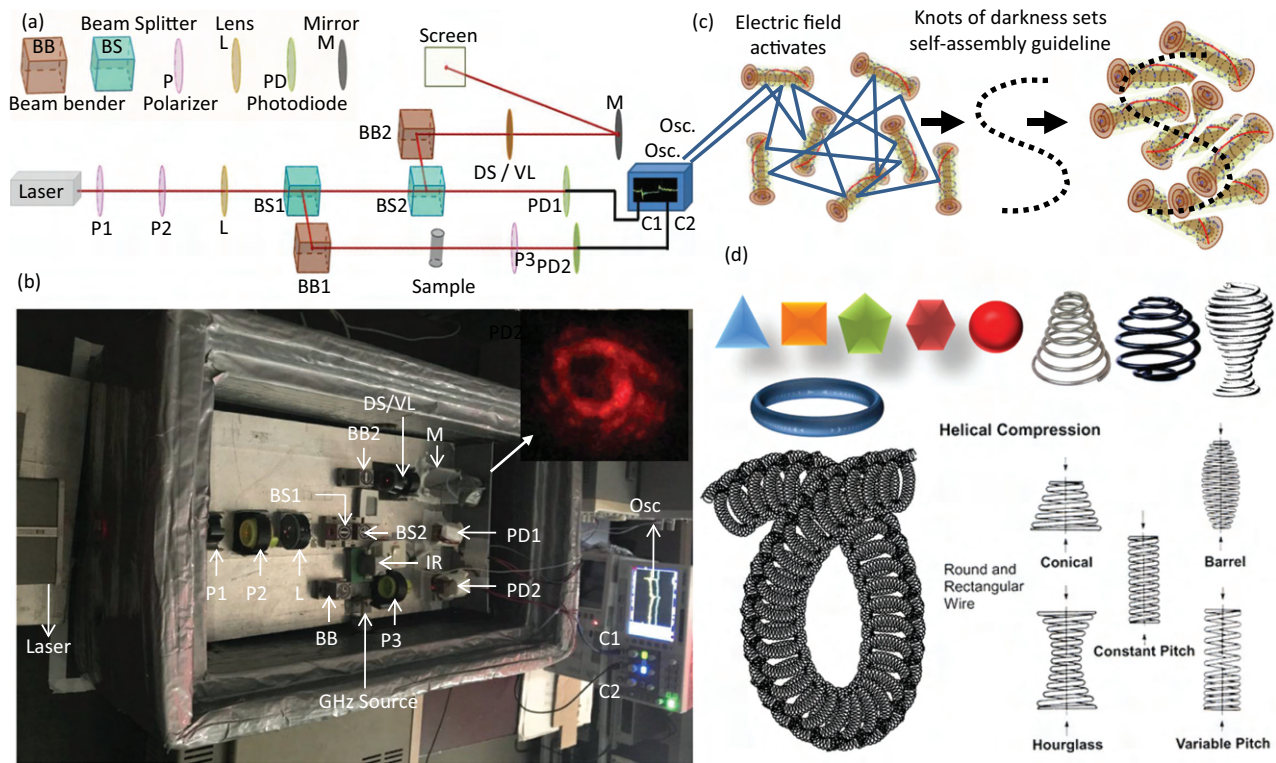


FIGURE 8.13 (a) Schematic and (b) actual experimental set up of quantum coincidence. Here, photons emitted by the polarized laser light (633 nm) are split using 50/50 beam splitter (BS1, HP 10701A 50% beam splitter). By splitting one of the 50% beam using 50/50 beam splitter (BS2), the coincidence effect of the two intensities is seen by high sensitive photodiode (PD1 and PD2). The output of this diode is observed in the oscilloscope (Osc.). Remaining 25% beam is used to see the vortex (VL) and double-slit (DS) images (with and without sample); inset shows an optical vortex. (c) The knots of darkness produced by different H devices form magnetic vortices and create a guideline for self-assembly which brings the H devices together. (d) Various types of geometric shapes are shown, their corner points are singularity points which bind together to form unique architectures.

arrives (multiwall helical nanotube), we get super-supercoil of magnetic field lines and so on. The approximate solution, when polarization is oscillatory $\Delta e = \sin \delta$, is two spirals, made of magnetic null or electric null, twisting each other. Together, they form a cylinder $r' = \Delta e/k = \sin \delta/k = \lambda \sin \delta/2\pi$, the pitch of the helix and the velocity of magnetic vortices are

$$\Delta z' = \frac{\lambda \sec \delta}{2} \begin{cases} < 0 \text{ right-handed} \\ > 0 \text{ left-handed} \end{cases} \dots \text{and velocity } v = c \sec \delta \quad (8.6)$$

Nature of harvested pure magnetic flux from light depends on the angle α made by perturbation wave from the inner and outer coil. At $\alpha < 0$, average intensity \bar{e} and polarization Δe both should be high (~2), to create a ring of electrical null, that is a magnetic ring along with hairpin-like electrical singularity or magnetic structures $\vec{\psi}_{mag}$. At $\alpha > 0$, even if there is no polarization ($\Delta e = 0$), even a low-intensity signal ($\bar{e} \sim 1$), generates a ripple-like magnetic structure (no hairpin) in a twisted helix. If α switches sign, the clocking direction changes. If both the inner and outer coil contributes together, $\vec{\psi}_{mag}$ holds a combination of clockwise and anticlockwise rotating rings produced from the same signal source in the central coil. If Δe varies periodically $\Delta e = \sin \delta$, then α switches sign periodically, we get a superposition of three patterns. Due to $\Delta e = \sin \delta$, the twisted spirals made of magnetic and electric dark lines are also created on the central coil. The super-super coil is shown in Figure 8.12d.

In principle, 2^{12} topologies could be created on the central coil governed by Hamiltonian \mathbf{H} , which links atomistic events to the blinking of cones, i.e., clocks that links G-mode to vortex atom made crystal $\sum_{i=1}^N C_i(r, t)$. By changing the color of reading light $\hbar\omega$, we could selectively project the phase spheres on the magnetic screen, read $\sum_{i=1}^N C_i(r, t)$, part by part. Then, by shifting the angle of incidence on the quartz cell, and pumping a GHz noise, we changed the beating caused by three identical concentric cylinders, thus concluded that beating amplifies B, enhances the magnetic field resolution in $P(r, t)$.

Seeing atomic-scale dynamics on a large film 5 m far from a nanostructure is a new marker, low-cost ambient spectroscopy (Figure 8.13b, inset). While optical vortices carry only the density of electrons on the surface, the magnetic vortices carry not just the geometric features, but the dynamics related to the symmetry breaking of multiple modes of vibrations of all three layers. The theory begins at the atomic scale, includes input em resonance and the light-matter interaction together with the unique roles of device geometry. Most importantly, one could wirelessly write the G-modes selectively on the device, which can memorize it, then erase, read and transport it to a long-distance, since a linear relationship between the stored charge and the magnetic flux produced holds true, widely. In an assembly, the G-modes of several H devices would get active and since the whole interaction process is wireless, a higher level assembly would trigger (Figure 8.12c).

8.6.3 MORPHOGENESIS OF KNOTS IN VORTEX-LIKE MAGNETIC ATOMS

All rings in the vortex are quantized: phase singularity of dark lines regulates geometric musical language (GML): topological charge: In the empty space, destructive interference of electromagnetic wave at nodal points is a phase singularity. Along a dark line, around linear phase singularity, the phase of reflected light from trapped charge site changes spirally around the singularity point. Some geometric shapes created by the topology of dark lines is shown in Figure 8.13d, this is how geometric musical language is implemented using H devices. To cover the distance of the electromagnetic wave, the number of times the topological charge rotates is the topological charge. The topological charge is the measure of the clocking charge on the surface of the coil in a Hinductor device. The number of dark rings with electrical null or magnetic vortex atoms generated during interference is a measure of the magnetic flux. The relation between charge and flux is constant. The magnetic ring looks like the vague attractor of Kolmogorov (VAK) that could model the stationary states of quantum mechanics (El Naschie, 2003). The relation between charge and flux is constant H. The physical significance of H is the inverse measure of singularity in an assembly of topological symmetries. Since a device could open or close the singularity holes in the phase sphere 4×10^3 ways, the magnitude of $H \sim 10^{-3}$. For each dimension of trapping cells on the coil surface, a distinct geometry of the magnetic ring is produced, with a distinct topological charge. Under noise, the sum of topological charges and the sum of magnetic rings produced are a function of a number of distinct types of cells the dimension of cells and the total number of cells on the surface.

Thus, in the electrical null, $E \neq 0$, rather $E_{ring} = E_{outside}/C^2$. Inside a ring, the velocity of field is $v = c \sec \delta$, where δ is the twist of the Hinductor coil, generating a mixture of the edge-screw defect. Now $\sec \delta = hv/hC = \phi/\phi_0$, thus, the dark rings are quantized, one cannot create rings of any arbitrary diameter. Quantization ensures the formation of distinct geometric shapes since the creation of an additional wave function $2\Psi_n^2 e^{i2\pi\phi_n/\phi_0}$ ensures a clocking interaction between discrete magnetic rings $\Psi_1, \Psi_2, \Psi_3, \dots$. A pair of rings separated by x and L are related by $\Psi_2(x+L) = e^{i2\pi\phi_2/\phi_0} \Psi_1(x)$. If Ψ_1, Ψ_2, Ψ_3 forms a triangle, with an angle between Ψ_1, Ψ_2 as $2\pi\phi_2/\phi_0$, then we get three angles among three hypothetical sides of a triangle. It is the basic geometric information creation for GML. In a closed ring of phase singularity, if an oscillating electric field is applied, a spatial gradient of the magnetic field is created, which clocks around the ring. We made a journey from lattice surface to the magnetic knot based geometric structures which one could read using magnetic vortices (Figure 8.14a). Using scanning tunneling microscopy images, one could map the distribution of charges on the fourth-circuit element surface and by pumping monochromatic polarized light see the magnetic vortices. The composition of circles is the time crystal we described as GML in Chapter 2.

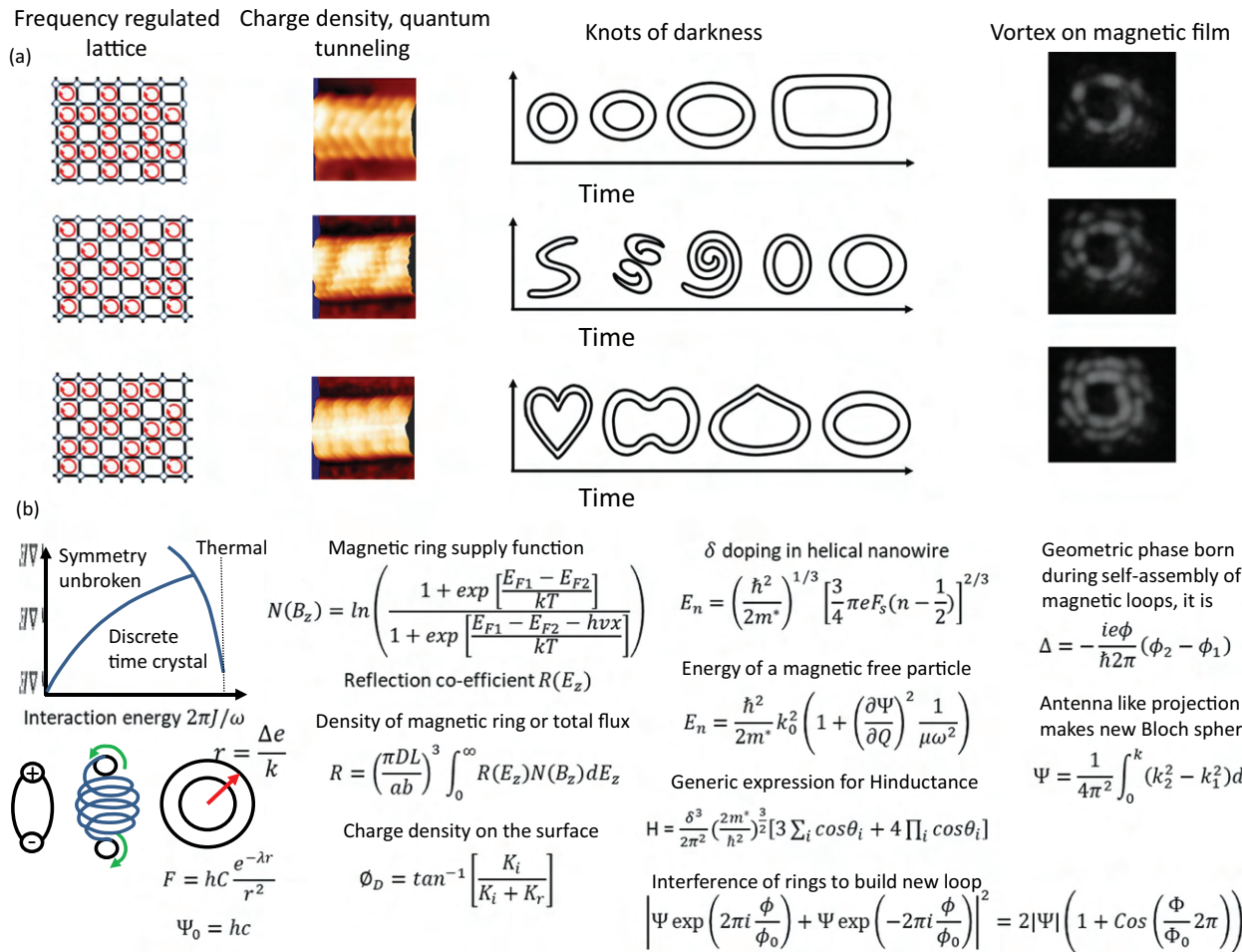


FIGURE 8.14 (a) A table showing density of charge on the surface of a microtubule and the knots of darkness, magnetic vortices. First column shows schematic of cells filled with charge and empty cells. Second column shows the STM images of the microtubule surface under the ac electromagnetic signal pumping. Third column shows the schematics for knots of darkness. Fourth column shows the magnetic vortex. (b) The top left plot shows the phase diagram for the time crystal. The horizontal axis shows the interaction energy between a pair of clocks and vertical axis shows the perturbation to the system. Three regions have been identified, a region where symmetry does not break, a domain where we see the time crystal. Just like electrical dipole magnetic dipole exists which has unique topology. All essential equations are compiled, terms are explained in the text.

8.7 MAGNETIC KNOTS' DRIVEN SELF-ASSEMBLY

Using a 3D distribution of such tubule-morphic H devices we can build a time crystal computer that is the artificial brain or nano brain or a brain jelly. Kids often play a game where they put a large number of magnets in a loop shape on a table and some others randomly within that loop. A small perturbation to that arrangement triggers self-assembly and all randomly distributed magnetics come together forming a linear assembly. The line of magnets resides along with the skeleton structure located inside the loop, one could write a program to build the skeleton of a shape and the magnetic would follow just that (Figure 8.13c). Getting aligned to the path set by the magnetic or electrical knots of darkness is the fundamental information processing mechanism of the artificial brain described here. Self-assembly of tubulomorphic devices builds artificial magnetic metamaterial like structure like neuromorphic devices (Baena et al., 2004). The self-assembly does not stop, it builds

neuromorphic devices, cortico-morphic devices as outlined in the 17 distinct brain morphic devices in Figure 9.2. One interesting discussion regarding the self-assembly of their biological counterparts is in Figure 7.11. Magnetic field driven the synthesis of helical superstructures is well studied system in the research field of synthetic chemistry (Singh et al., 2014). However, in this particular case the self-assembly is driven by phase shifts and fine tuning of the negative refractive index of the elementary H devices during self-assembly process (He et al., 2007). The brain jelly or the key computing organic material is not made of switch-like devices, which would be H here. During the course of structural synthesis, from basic precursors H devices grow, even asymmetry in mechanical vibration like sound could regulate the artificial magnetic metamaterials, which are basically a composition of different metamaterials, i.e., with different refractive index and magnetic permeability (Wang et al., 2014b).

Synthesis of protein-like structure using helical carbon nanotubes is quite common in materials science (Grigoryan et al., 2011), in the assembly they do not go for liquid crystalline features rather grow further. One of the prime objectives of Hinductor based brain jelly synthesis is that helical superstructures would build up naturally (Nakashima et al., 2005). Hinductor or fourth-circuit elements are to be synthesized in the solution under the presence of an input signal (Wang et al., 2014a). Helical superstructures are often synthesized for the directed reflection or formation of directed light. Not just directed light, we could control even the light reflected, filtering frequency (Li, 2012). Polarization direction and typical features of polarization are also detected using helical nanowires. Polarization direction and typical features of polarization are also detected using helical nanowires (Mathews et al., 2010). Even the structures change when light falls onto a system (Bisoyi and Li, 2016). The particular feature is very useful for hierarchical spontaneous information-driven growth for the synthesis of brain jelly from nanowires. Lattice-based photo-tuning by self-organized superstructures (Qin et al., 2018) are found extensively reported in the literature.

The physical realization of a quantum clock to build a quantum time crystal: The difference between quantum and fractal time crystal? This book explores the possibility of a fractal time crystal spread over 12 imaginary worlds, it could have a classical or a quantum version. We have summarized several basic physical situations encountered in the time crystal exploration in [Figure 8.13b](#). The idea is to make the reader visualize how very well known school level quantum studies contribute to the new understanding of time crystal with a twist. A quantum clock satisfies two types of constraints—first is bound on the time resolution of the clock which provides by the difference between the minimum and maximum energy eigenvalue; another one is Holevo's bound which tells about how much classical information can be encoded in a quantum system. In this work explains results such as optimal quantum clock using trapped ions (Buzek et al., 1999). As the [Figure 8.14b](#) explains the phase diagram of a large number of clocks working as a single system (Khemani et al., 2016). There are three domains; when an interaction between the participating clocks (e.g., spins of an array of electrons) is very low, symmetry does not break and if the energy is more then thermalization breaks the coupling between the clocks. In between the two limits there could be a new phase of matter in the pre-thermal regime which is protected by discrete time translation symmetry (Else et al., 2016, 2017). The clock assembly breaks time symmetry and automatically regenerates it. If the quantum ground state is essential, then quantum mechanically no one could realize a quantum time crystal (Bruno, 2013). The demand for quantum time crystal is beautiful ([Figure 8.14b](#), top left), there is a thermodynamic restriction, once measurement is done the system would not remain in the universal ground state, for complete and autonomous measurement, the clock or periodically oscillating system must find a meta-ground state so that later, post-measurement the system returns to the universal ground state (Erker et al., 2017). The space-time could be symplectic, i.e., differentiable,

geometric (measure length and angle; McDuff and Wehrheim, 2012), some of the quantum clocks are same as which characteristic of broken symmetry and topological order and other are new which characteristic by order and non-trivial periodic dynamics. In simple words, slow down the energy exchange process finding cool imaginary ideas (Peres, 1980). Quantum has only one imaginary world, so it is difficult to keep imaginary relation intact and still switch between global minima and excited state. Quantum time crystal (Wilczek, 2012) is impossible, such an argument has valid points (Watanabe and Oshikawa, 2015) in spite of prescriptions on how to build a practical time crystal (Yao et al., 2017) and subsequent claims to realize the same. In this book, 12 imaginary worlds layered one inside another achieves one incredible feature a higher topology of clocking between the imaginary world ($2 \times 2 \times 3$, $2 \times 3 \times 2$, $3 \times 2 \times 2$) that feature has the ability to hold on to a time crystal. Just dumping noise to higher-dimensional worlds is not enough; only then one could achieve a truly autonomous machine (Woods et al., 2016).

8.8 DESIGN APPLICATION AND OPERATION OF H—THE NOVELTY OF H

[Figure 8.15](#) outlines Hinductor's journey with applications, where should we use such a device, while [Figure 8.16](#) outlines the novelty of this device.

- 1. A linear array of capacitors forming an inductor: edge and line dislocations on the lattice are required:** We need capacitor like extreme charge storage devices to arrange in the form of a spiral or vortex or fractal so that no current flows. Either leakage current, or soliton or electromagnetic wave propagating through the surface would interfere with the geometric boundaries and would create an electron density distribution analogous to the charge stored on the surface. Current and voltage have no effect on this device. So, we get only two variables of magnetic flux and stored immobile charge.
- 2. The ratio of helical pitch and diameter a pure geometric variable would determine it band or electronic/optical property:** Helical magnets or helical distribution of magnetic flux changes magnetic property very differently, that's why super-super helices would be a fascinating geometric phase architecture to look into (Katsura et al., 2007; Ishiwata et al., 2008). The helicity of the geometry is a robust concept, helical does not always mean to be a cylinder-like spring. Growth/decay of helical conducting path with the storage of charge depends on a geometric parameter P . The ratio of helical pitch to the radius of helix is P , P and the dielectric constant ϵ of the helical path, control the fundamental features of φ - q relationship. By tuning P and ϵ , one can modulate signal amplification and energy storage features of H. Due to the periodicity of a helix and quantized charging it tunes the electromagnetic energy very

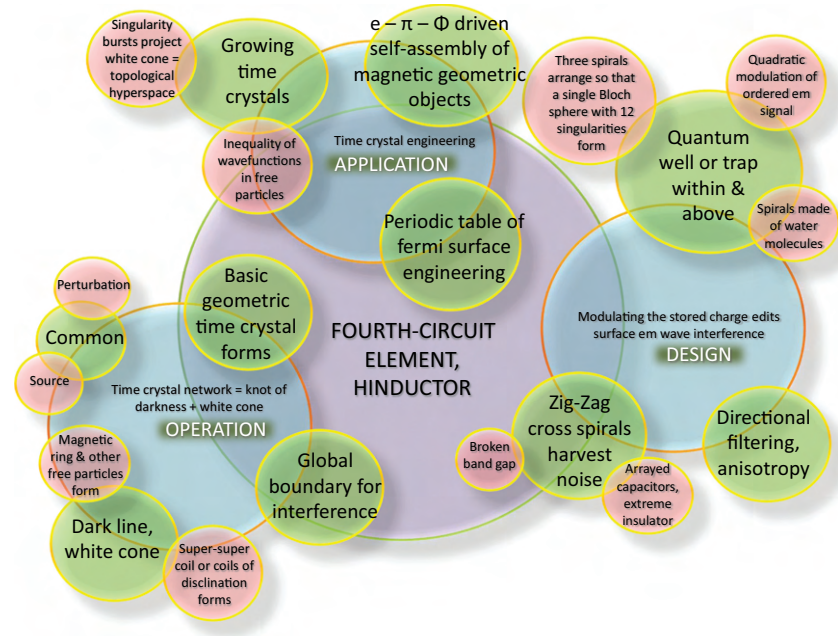


FIGURE 8.15 A summary of the fourth-circuit element fundamentals for the industrialization.

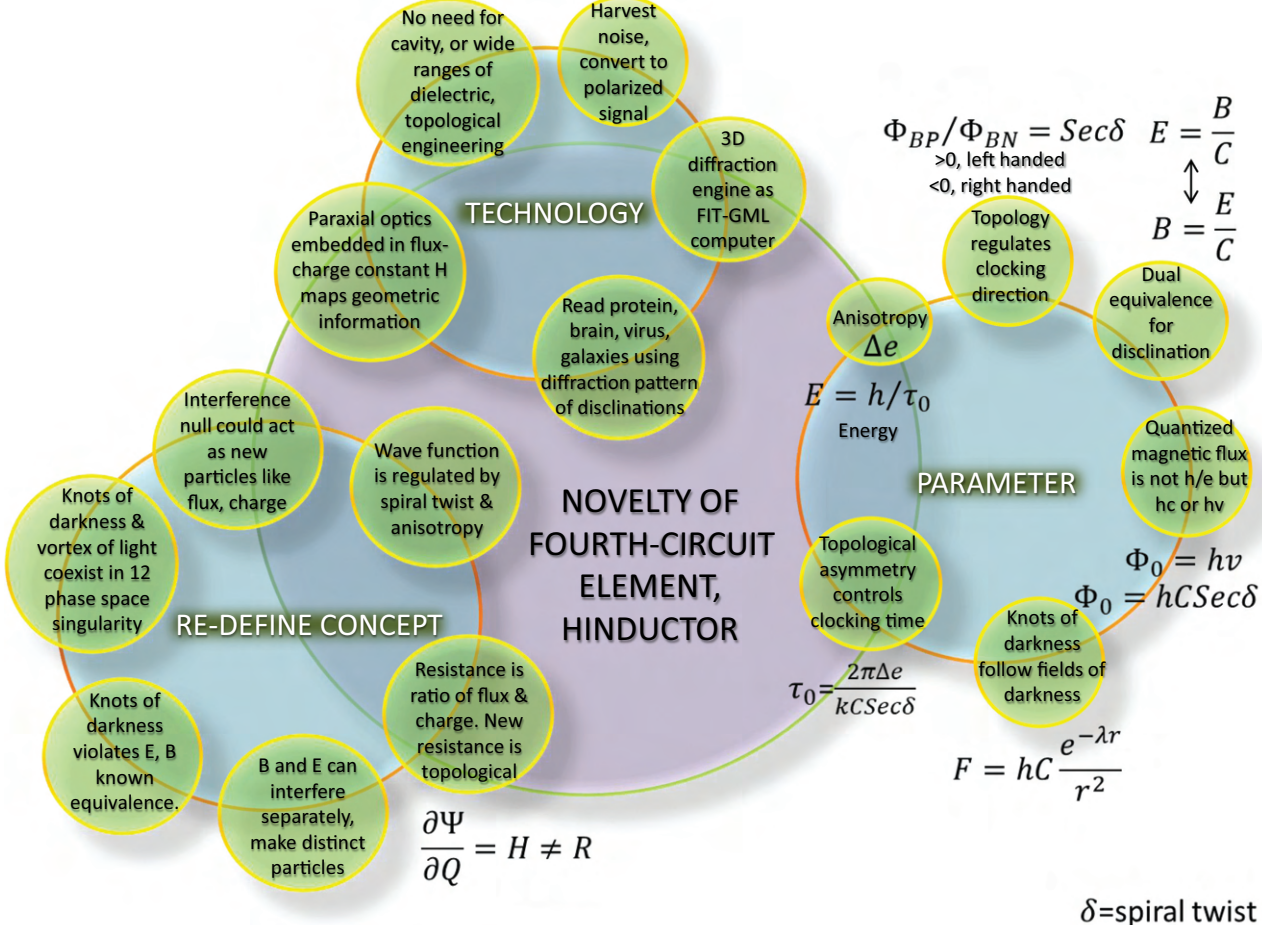


FIGURE 8.16 Novelties of the fourth-circuit element.

accurately. By modifying the helical pitch, one can change the quantization features. Lattice cells are key charge oscillating center. One should be able to write a pattern of charge distribution by changing the geometric parameters of the device. One possible route could be pumping a composition of ac signal wirelessly.

3. **Operational between upper and lower bound frequencies:** Though there are no real capacitor and inductor in the device, we may consider rapidly oscillating dielectric centers as capacitors and spiral pathway induced anisotropic transmission as an inductor. Capacitors are simply dielectrics; bonding between multiple capacitors also behave as electric dipoles. Simply by changing the material composition if two parameters (i) threshold frequency of the capacitor and the (ii) threshold frequency of the inductor are tuned by modifying the architecture, then capacitance and inductance values of the materials are changed. It is possible to tune these values to change the threshold frequencies. The capacitance determines the lower limit and inductance determines the upper limit of the bandpass frequency. If inductor L and capacitor C are fused, by constructing the inductor by linearly connected capacitors then for the new element H we get much faster response against load R . Here is the mathematical proof: Though R , C , and L cannot generate H , for the relative comparison we construct a simplified current expression for H . Tubulin dimers are charged following $Q = Q_0(1 - \exp(-t/CR))$ and as $Q \propto L$, we get $L = L_0(1 - \exp(-t/CR))$. The current grows in the inductor following $i = i_H(1 - \exp(-tR/L))$, therefore the current in an H grows following equation $i = i_H(1 - \exp(-tR/L_0(1 - \exp(-t/CR))))$ and decreases following $i = i_H(\exp(-tR/L_0(\exp(-t/CR))))$. Considering C dominating current, we get current growth as $i = i_H(1 - \exp(-t/RC_0(1 - \exp(-Rt/L))))$. It is much faster than any resistor, capacitor or inductor.
4. **Topological properties for asymmetric absorption of electric and magnetic vectors:** Recently, the synthesis of helical nanotubes and rosette structures has received wide attention; one ripple effect is the creation of extensive theories on helical electronics. In a cylindrical conductor, the injected 2D electron gas from one end distributes in a helical symmetric pattern on the surface due to polarization. The electron density peaks are periodic along the length. In a helical nanotube, the bandgap closes at a point called Fermi contact point if the conductivity is low or is semiconducting in nature. However, the gap closes at more point contacts if the conductivity turns metallic, which enables the system to exhibit coherent transport at a particular condition. When the current flows through a helical nanotube, Fermi contact point acts as a gating channel and enables quantized transport of charge. It is a situation similar to the creation

of a fractured band. H by nature will be an insulator and the geometric path would determine its key carrier transmission, therefore, we have simulated the power usage of this device, which ranges in the domain atto-watt to femto-watt (picoampere, microvolt). Spiral current also generates a magnetic flux only at certain frequencies, which shifts the entire band of energy levels equal to the number of quantized magnetic flux (Φ/Φ_0) in the k space, enabling H to store energy.

5. **Phase quantization:** When ac signal flows, it changes the polarization of signal, we cannot trigger charge to move in one direction, thus we cannot generate a finite magnetic flux. Therefore, we need an ac signal on a dc background. Obviously, we need two simultaneous additional control parameters ac frequency and a dc bias to release charge and generate magnetic field unlike conventional L and C where only ac or dc signals are sufficient to generate the basic property. When ac signal is maximum it is absorbed by dielectric molecules of the capacitors, the current output is zero and when it is minimum, carriers are released and the current output is maximum. The output signal is therefore always 180° out of phase from the input signal.
6. **Quasi-particles: Ultra-low power device:** If the embedded spring of the spiral architecture expands/contracts, the structural symmetry breaks, Dirac points split and the bands in point-contact are separated. However, if the symmetry is restored, the degeneracy appears, and the two-phonon bands touch at distant points. Thus, point-contacts of Dirac gates open and close continuously—a perpetual interplay of soliton fractions between two limits unravels how a purely mechanical (phonon) transport of energy safeguards pure electronic signals even when noise is more than the processing signal. In the learning⁴ phase, solitons are locally synchronized, microtubule accepts input signal/noise, corrects errors by tuning soliton fraction. It operates in a very low power domain (nano-watts), etc.
7. **Ferroelectric, piezoelectric and pyroelectric behavior:** A single spiral structure's perfectly square or lossless hysteretic current-voltage (IV) characteristic depicts an ideal ferroelectric memory switching (Sahu et al., 2013a), where hysteresis area is a function of maximum applied bias/current. The device does not flow current, entire response is related to leakage current and voltage induced dipole moment switching of the cells. It has been demonstrated live that in a nanowire, if the constituent dipoles made of proteins switch in a regular manner then conductivity switches as observed in the current-voltage characteristics. Since the spiral's ferroelectricity leads to its piezoelectric and pyroelectric features, it oscillates like a spring between two limiting lengths.

- 8. Strong anisotropic elastic properties: resonance frequency in the ratio of primes:** Thus, it is tested and verified that these devices are subjected to strongly anisotropic elastic properties; it was proved that longitudinal bonds along the protofilaments are stronger than lateral bonds between adjacent protofilaments. Simply by calculating the longitudinal modes, it has been found that vibration would decrease by 1000 times than its dipole-based calculated values. Later, rigorous orthotropic shell model-based studies, which included anisotropy in a more generic 2D shell-like hollow structure of these spiral architectures only reproduce experimental observations, even if we do not include the transverse sheering. If the small-scale effect of non-local elasticity is introduced, which considers that local strain is the collective output of global force, the result hints at 10,000 times lower time-domain resonant oscillations. However, on this concept, when circumferential mode or local radial strain is included, the vibration onset frequency is reduced by 100,000 times. Thus, depending on typical modes, the spiral's resonance ranges from a few kHz to MHz to GHz, which means 1:1000000 times bandwidth variation is observed. Most strikingly, since 12 holes in the phase space blink, the resonance frequencies burst like an antenna.
- 9. Quantum cloaking:** We are aware of the electromagnetic cloaking, where the light bends around a device. It may also be possible that by pumping a vortex or spiral, one could resonate a dielectric material electromagnetically. At resonance, matter wave passes through like a lens. It is quantum cloaking. Using an H device, one could pump suitable ac frequency signal using an antenna and simultaneously scan the material using a scanning tunneling microscope, the tunneling image would show vanished material, the empty surface. If we have three-layered helices or vortices or multi-fractals, then we could selectively vanish a part of the material using a suitable ac pumping frequency.
- 10. Wireless communication between similar devices:** H transmits electromagnetic signals of a particular frequency (we call it resonance frequency), this passage causes electromagnetic oscillation in the structure, it might affect the associated mechanical vibration-induced conformational changes, which could shift the resonance frequency. By suitably combining the spiral structures of different lengths one could generate the desired resonance band. There are three parts in the resonance band of any seed oscillator structure, one part is kept open for coupling with the next seed that will be formed after the self-assembly, one part is for its own processing, and the third part couples with the resonance bands of the seeds inside the structure. Thus, every seed

H device has two hands in the resonance spectrum. Synchronization could trigger with one or more peaks singular or in a plural manner in the system. The capacitor molecular structures in the 2D hollow cylindrical mesh act as an evolving circuit at resonance frequencies in such a way that it works as an antenna and also a receiver for wireless and lossless electromagnetic power transmission. The brilliance of this wireless transmission is that (i) a sender nanowire device automatically selects a suitable receiver nanowire for the maximum power transmission in a bundle, because there is a quantum cloaking at the molecular scale; communication is classical, but quantum cloaking enables the atomic-scale molecular property to reveal itself, (ii) even by wirelessly sending a part of a time crystal code, an entire information packet could be transmitted, (iii) the operational power could automatically be amplified during a “communication avalanche.” Such a massive scale power transmission is not just lossless, rather creates an additional power logically as required in the receiver, which has always been considered impossible in the conventional communication engineering. The sender does not send much power; the receiver fills the canals once it receives the code.

8.9 TRANSITION FROM THE OLD ERA OF ELECTRONICS TO MODERN MAGNONICS

There existed a world of superconductors. There will be a world of super non-conductor giving everything that superconductor gives. It does not transmit electron, but a phase in terms of quasi-particle propagates through the surface and interacting with the transmitted waveform (Sun et al., 2012). Metamaterials are widely used for analog computing, performing mathematical operations using sound waves (Silva, 2014; Zuo, 2017), solving differential equations and integration (Abdollahramezani, 2017), often data is encrypted by geometric phase by modulating the surface (Biener et al., 2005). This is now a journey from collision to coexistence, rejection to live together, magnitude to look (Figure 8.17). Two features make a significant difference in the cultural transition where a mechanics used multi-meter to solve any electronics problem, to the world where they would use a semiconductor camera to measure magnetic flux pattern. How the world would change is outlined in Figure 8.18.

Hologram generated by metamaterial: advanced computing harvesting metamaterial surface: Quadratic $e - \pi - \phi$ control on the resonance, cloaking and holographic projection: We are all aware of phase hologram; it has become a tool for the entertainment industry. Hologram and the time crystal-based GML has an intimate relationship. When a cube is inserted inside a phase sphere, its eight points touch the spherical surface. No image is captured by

	Current-voltage paradigm	Charge-flux paradigm
Transmits	Current (I)	Magnetic flux (ψ)
Potential driver	Voltage (V)	Charge(Q)
Resistance	$R = V/I; H = \infty$	$H = \psi/Q; R = \infty$
For Capacitor	$R = \infty$	$H = \text{finite}$
For Inductor	$R = 0$	$H = \text{finite}$
Conductance	$G = \partial I/\partial V$	$K = \partial Q/\partial \psi$
Qu. capacitance	Gt	$f(\text{density of states})$
Qu. inductance	$G^{-1}\tau$	$f(\text{density of states})$
Energy	$I^2R; CV^2; LI^2$	$Q\psi$
Derivation	$R = \rho L/A; C = \epsilon A/d; L = \mu nI$	
Phase change	Between I and V, $R=0, C=+90, L=-90$	Between ψ and Q, $H = 0, \pm\pi$
Quant Conductan.	$G_0 = 2e^2/h$	function of phase space topology
Quant flux	$\Phi = h/2e$	function of phase space topology
Regulator	Scattering, collision	Repeated reflection, clocking
Charge, spin	Charge (e, e-p, ne), e/n. Spin (p/q, fraction)	Charge, Spin function of phase space topology
Power	$P = I^2R$	$P = \psi^2Q$
Resonance	$\omega \sim 1/\sqrt{LC}$	function of phase space topology
Current-voltage	Yes, linear for R, no for C and L	No for H
Flux-charge	No if R, L and C are separate.	Yes for H, if $Q(\psi)$. LC if $\psi(Q)$

FIGURE 8.17 A table is comparing the existing current-voltage paradigm existing today and the charge-flux paradigm that is going to come soon.

Memristor	Hinductor	Old electronic	Magnonics
Have current voltage, IV feature	Does not flow current, flows rings of Ψ		
Helical current generate magnetic flux	Flux generates by asymmetric treatment of em wave	Vortex around defect, spin ice	Look alike of a monopole, can be used at RT
Unit: resistance, R	Unit: inductance, H; resistance= ∞		
Topology has no role	Topology governs H	Dark lines are neglected	Dark line holds novel concepts
2 terminal device, a sandwich structure, semiconductor	0/n terminal, spiral array of insulators & semiconductor/metals	Tune electric field to generate force for synthesis or self-assembly.	Tune magnetic particle geometries so that in an electric field they build structures.
Noise disrupts operation	Harvests noise		
No perturbation required	Three layers with similar helical symmetry to create free magnetic particles		
Wide ranges of IV unit, transistor, amplifier, filter	Wide ranges of Q Ψ unit, transductor, amplifier and filter	Fixed boundary conditions	Unstable, rapidly vibrating undefined boundaries.
Wiring needed	Wireless 3D orientation		
Energy transfer, power needed	Symmetry transfers, rebuilds information	Only one imaginary world in quantum	Layers of imaginary worlds and even they interact and integrate.
Need e insulating shield,	Need metamaterial shield for em wave.		
Transmits one frequency	Processes time crystal, many frequencies		
Low temp for superposition	RT superposition by coexisting lattices		
Wire freely, objective: function	Assemble only by fractal symmetries	Regulates conductivity not topology	Harvest singularity Extreme insulator

FIGURE 8.18 Table left, Existing fourth-circuit element memristor and Hinductor, a comparison. Table right, Old world of electronics and the future world of magnonics.

the device, rather some key points of a geometric shape are morphed as is in a 3D space, phase relationships between different points are preserved, this is exactly what a hologram does, a bit differently (Cathey, 1970). Thus, A geometric-phase shift is added as a “memory” to the angular momentum of light through anisotropic parameter space. A hologram could be made of sound (Xie et al., 2016), light, heat or thermal (Larouche et al., 2012) and magnetic field (Mezrich,

1970). Even water wave cloaks (Yang et al., 2016). Thus, electric, magnetic and mechanical resonances coupled by $e - \pi - \phi$ quadratic relationship would exhibit cloaking when necessary and generate holographic projection when necessary. Holograms always have an intimate relationship with the helices and vortices (Huang et al., 2013a, 2013b).

Electromagnetic cloaking, magnetic cloaking, and acoustic cloaking: Cloaking means light bends through a

material and returns to the original path (Pendry et al., 2006; Schurig et al., 2006). What could bend? Ions could bend if the structure is cylindrical; since microtubule inspired Hinductor devices are cylindrical, they could turn invisible if anyone tries to see them using ion flow, even axons of a neuron or DNA could cloak with ions. Electromagnetic waves could exhibit cloaking, theoretical studies show that at two distinct frequency bands exist between 6 and 25 GHz where the material exhibits cloaking. It needs to be checked if microtubule or other fourth-circuit elements also exhibit cloaking

for audible acoustics, then sound or mechanical waves would pass through (Faure et al., 2016). At ac resonance condition, it is also possible to deliver a magnetic cloaking (Zhu et al., 2015). As it has been described above, electric, magnetic and mechanical resonances are coupled by $e - \pi - \phi$ quadratic relationship. Therefore, a quadratic cloaking by three simultaneous modes would ensure electrical signal induced power supply, the magnetic field induced information transport and mechanical force-induced hardware evolution simultaneously.